UC-4
LBL-17447
Preprint c.1

Lawrence Berkeley Laboratory

UNIVERSITY OF CALIFORNIA

RECEIVED
LAWRENCE
BERKELEY LABORATORY

MAY 30 1984

LIBRARY AND
DOCUMENTS SECTION

Materials & Molecular Research Division

Submitted to the Journal of Chemical Physics

UV PHOTODISSOCIATION OF C_2F_5Br, C_2F_5I AND 1,2-C_2F_4BrI

D. Krajnovich, L. Butler, and Y.T. Lee

April 1984

For Reference

Not to be taken from this room

LBL-17447 c.1

Prepared for the U.S. Department of Energy under Contract DE-AC03-76SF00098

DISCLAIMER

This document was prepared as an account of work sponsored by the United States Government. While this document is believed to contain correct information, neither the United States Government nor any agency thereof, nor the Regents of the University of California, nor any of their employees, makes any warranty, express or implied, or assumes any legal responsibility for the accuracy, completeness, or usefulness of any information, apparatus, product, or process disclosed, or represents that its use would not infringe privately owned rights. Reference herein to any specific commercial product, process, or service by its trade name, trademark, manufacturer, or otherwise, does not necessarily constitute or imply its endorsement, recommendation, or favoring by the United States Government or any agency thereof, or the Regents of the University of California. The views and opinions of authors expressed herein do not necessarily state or reflect those of the United States Government or any agency thereof or the Regents of the University of California.

LBL-17447

UV PHOTODISSOCIATION OF C_2F_5Br, C_2F_5I AND 1,2-C_2F_4BrI

D. Krajnovich,* L. Butler, and Y. T. Lee

Materials and Molecular Research Division
Lawrence Berkeley Laboratory and
Department of Chemistry
University of California
Berkeley, California 94720

April 1984

This work was suported by the Director, Office of Energy Research, Office of Basic Energy Sciences, Chemical Sciences Division of the U.S. Department of Energy under Contract No. DE-AC03-76SF00098.

*Present address: Department of Chemistry, Indiana University, Bloomington, IN 47405

UV PHOTODISSOCIATION OF C_2F_5Br, C_2F_5I AND 1,2-C_2F_4BrI

D. Krajnovich, L. Butler, and Y. T. Lee

Materials and Molecular Research Division
Lawrence Berkeley Laboratory and
Department of Chemistry
University of California
Berkeley, California 94720

ABSTRACT

The photodissociation reactions of C_2F_5Br, C_2F_5I, and 1,2-C_2F_4BrI have been studied at 248 and 193 nm using the crossed laser-molecular beam technique. Photodissoiation of 1,2-C_2F_4BrI was also studied at 266 nm. We find that: (i) C_2F_5Br undergoes C-Br bond fission at 193 nm (but does not absorb at 248 nm); (ii) C_2F_5I undergoes C-I bond fission at 248 nm (but does not absorb at 193 nm); (iii) 1,2-C_2F_4BrI undergoes only C-I bond fission at 248 nm + 266 nm, but at 193 nm both C-I and C-Br bond fission are observed, with a C-I:C-Br fission ratio of approximately 1.7:1. Center-of-mass recoil energy and angular distributions were determined for each of these photodissociation reactions. These results, combined with those of other workers, are used to test simple predictions based on molecular orbital theory. The 266 nm data for C_2F_4BrI provide an approximate value of 19.3 $\pm$ 3 kcal/mole for the dissociation energy of C_2F_4Br to C_2F_4 + Br and also show that all or almost all the iodine produced in the primary C-I bond fission is excited state. The prospect of doing bond-selective photochemistry in the ultraviolet discussed.

UV PHOTODISSOCIATION OF C_2F_5Br, C_2F_5I AND 1,2-C_2F_4BrI

I. INTRODUCTION

In the 1930's, Mulliken studied and compared the electronic structures in the ground and low excited states of a variety of molecules using the molecular orbital method.[1] In particular, detailed studies of the halogens (X_2, XY)[2], hydrogen halides (HX),[3,4] and alkyl halides (RX)[5] were carried out. These studies led to the first interpretation of the UV absorption spectra and ionization potentials of halogen-containing molecules. Subsequent experimental and theoretical work has tended to confirm the correctness of Mulliken's basic ideas and conclusions.

Mulliken mainly followed the Lennard-Jones procedure of assigning unshared electrons to atomic orbitals (A.O.'s), and shared electrons to molecular orbitals (M.O.'s). In the halogen atoms, one of the five valence p electrons can be shared to form a chemical bond, while the other four p electrons are expected to be essentially non-bonding. With this assumption, the lowest energy electron configurations and ground state symmetries of X_2 and HX may be written as:[2]

$$X_2: \ldots (np\sigma + np\sigma, \sigma_g)^2 (np\pi)^4 (np\pi)^4, \ {}^1\Sigma_g^+ ;$$

$$HX: \ldots (n_x p\sigma_x + s_H, \sigma)^2 (n_x p\pi)^4, \ {}^1\Sigma^+ ,$$

where n = 2, 3, 4, 5 for X = F, Cl, Br, I. (The ns halogen electrons, as well as electrons inside the valence shell, have been omitted). $np\sigma$ and $np\pi$ denote the p electron A.O.'s of the halogen atom. In X_2, the $np\sigma$ A.O.'s of the two halogen atoms combine symmetrically to give a bonding σ_g M.O. In HX, the $n_x p\sigma_x$ A.O. of the halogen atom combines with

the s_H A.O. of hydrogen to give a bonding M.O. In both cases, the $np\pi$ electrons are assumed to be completely non-bonding, as discussed above, and are left in $np\pi$ A.O.'s.

The lowest excited states of X_2 and HX are obtained by removing an electron from the highest $np\pi$ A.O. and adding it to an excited orbital. The lowest excited orbital should be the important anti-bonding σ^* orbital ($np\sigma - np\sigma$, σ_u^*) of X_2 or ($s_H - n_x p\sigma_x$, σ^*) of HX.

$$X_2: \ \sigma_g^2 \ \pi^4 \ \pi^3 \ \sigma_u^*, \ {}^{1,3}\Pi_u \ ;$$

$$HX: \ \sigma^2 \ \pi^3 \ \sigma^*, \ {}^{1,3}\Pi \ .$$

In Ref. 3, Mulliken gave the generic name "Q-complex" to this ${}^{1,3}\Pi$ complex. In both X_2 and HX, only the components ${}^3\Pi_1$, ${}^3\Pi_{0^+}$, and ${}^1\Pi_1$ (labelled ${}^3Q_1$, ${}^3Q_0$, and ${}^1Q_1$ by Mulliken) can combine radiatively with the ${}^1\Sigma_g^+$ normal state (N). The ${}^3Q_1$ <- N and ${}^1Q_1$ <- N transitions should be polarized perpendicular to the internuclear axis ($\Delta\Omega = 1$, where Ω is the component of the total electronic angular momentum along the internuclear axis), while ${}^3Q_0$ <- N should be polarized parallel to the internuclear axis, ($\Delta\Omega = 0$). Mulliken argues that ${}^3Q_1$ and ${}^1Q_1$ should correlate to ground state atomic products [$X_2({}^3Q_1, {}^1Q_1) \rightarrow X({}^2P_{3/2}) + X({}^2P_{3/2})$, $HX({}^3Q_1, {}^1Q_1) \rightarrow H({}^1S) + X({}^2P_{3/2})$], while ${}^3Q_0$ should lead to one spin-orbit excited halogen atom [$X_2({}^3Q_0) \rightarrow X({}^2P_{3/2}) + X({}^2P_{1/2})$, $HX({}^3Q_0) \rightarrow H({}^1S) + X({}^2P_{1/2})$].

These qualitative predictions have been born out by experiment. In the halogens, ${}^3Q_1$ and ${}^3Q_0$ are the well-known $A^3\Pi_{1_u}$ and $B^3\Pi_{0_u^+}$ states. Magnetic circular dichroism (MCD) has been used successfully to resolve the individual contributions of the $A^3\Pi_{1_u}$, $B^3\Pi_{0_u^+}$, ${}^1\Pi_{1_u}$ <- $X^1\Sigma_g^+$

transitions to the absorption spectra of I_2, Br_2 and Cl_2.[6] The parallel B <- X transition is by far the most intense in I_2, but decreases in intensity relative to $^1\Pi_{1_u}$ <- X on going form I_2 to Br_2 to Cl_2, due to weaker spin-orbit coupling in the lighter halogens.[7] The $^1\Pi_{1_u}$ <- X intensity is roughly constant in the three molecules, as would be expected for a fully allowed transition.

In the case of I_2 and Br_2, direct measurements of the yields of $^2P_{3/2}$ and $^2P_{1/2}$ halogen atoms following irradiation at selected wavelengths have been performed using the methods of molecular beam photofragment spectroscopy[8,9] and resonance absorption spectroscopy.[10-12] The photofragment spectroscopy experiments confirm that $^2P_{3/2}$ + $^2P_{1/2}$ products are formed via the parallel B <- X transition, while $^2P_{3/2}$ + $^2P_{3/2}$ products are formed in the perpendicular A <- X and $^1\Pi_{1_u}$ <- X transitions. Thus, the $^2P_{3/2}$:$^2P_{1/2}$ product ratio (as a function of wavelength) allows the strength of the B <- X transition relative to the (combined) strengths of the A <- X and $^1\Pi_{1_u}$ <- X transitions to be determined. The results of the photofragment spectroscopy and resonance absorption spectroscopy experiments agree reasonably well with the MCD results.

There has been much less experimental work on the hydrogen halides than on the halogens. The first UV continua of HI, HBr and HCl are broad and featureless, peaking around 220 nm, 180 nm, and 155 nm, respectively.[13] Clear, Riley and Wilson[14] studied the photodissociation of HI at 266 nm using the method of photofragment spectroscopy. They found that 36% ± 5% of the I atoms are formed in the excited $^2P_{1/2}$ state via a parallel transition, while the ground state I($^2P_{3/2}$) atoms are

formed via a perpendicular transition. These results are consistent with Mulliken's interpretation of the first HI absorption continuum in terms of overlapping transitions to $^3\Pi_1$, $^3\Pi_{0^+}$, and $^1\Pi_1$ excited states.

Finally, we turn our attention to the alkyl halides. Mulliken's molecular orbital considerations[5] suggest a close analogy between the normal and low excited states of the alkyl halides and the simpler halogen and hydrogen halide molecules. In particular, the highest occupied orbital in the normal states of the alkyl halides should again correspond to an essentially non-bonding $p\pi$ orbital on the halogen atom, and the lowest energy electronic transitions should correspond to excitation of one of these non-bonding p electrons to an anti-bonding σ^* molecular orbital on the adjacent carbon-halogen bond. Mulliken writes the electron configuration of the normal state of methyl iodide as:

$$CH_3I: \quad [sa_1]^2[\pi e]^4[\sigma a_1]^2(5p\pi_I e)^4, \ ^1A_1.$$

(The 1s carbon electrons, 5s iodine electrons, and electrons inside the iodine valence shell have been omitted). The bonding M.O.'s are shown in square brackets. The symbols a_1 and e tell to what representation of the point group C_{3v} the various orbitals belong. To a first approximation, the $[sa_1]$ and $[\pi e]$ M.O.'s may be thought of as being formed from three of the four carbon sp^3 hybrid A.O.'s and the three hydrogen 1s A.O.'s, while the $[\sigma a_1]$ M.O. is formed from the remaining carbon sp^3 A.O. and the $5p\sigma$ A.O. of the iodine atom. Although, in reality, $[sa_1]$ will have some C-I bonding character, and $[\sigma a_1]$ will be partially delocalized over the CH_3 group, it is still convenient to think of $[sa_1]$ and $[\pi e]$ as C-H bonding orbitals, and of $[\sigma a_1]$ as the C-I bonding orbital. The most weakly bound electrons in CH_3I reside in the $(5p\pi_I e)$ A.O. of

iodine. Excitation of one of these non-bonding electrons to an anti-bonding σ^* M.O. on the C-I bond gives the excited states

$$[sa_1]^2[\pi e]^4[\sigma a_1]^2(5p\pi_I e)^3[\sigma^* a_1],\ {}^{1,3}E\ .$$

${}^{1,3}E$ represents the "Q-complex" for CH_3I. As in the halogens and hydrogen halides, spin-orbit coupling causes the Q-complex to split into five components,[15] three of which (${}^3Q_1$, ${}^3Q_0$, ${}^1Q_1$) can combine radiatively with the normal state. Again, ${}^3Q_0$ should correlate to $I({}^2P_{1/2})$, while ${}^3Q_1$ and ${}^1Q_1$ should correlate to $I({}^2P_{3/2})$. Gedanken and Rowe[16] resolved the contributions of these three excited states to the n -> σ^* continuum of CH_3I using the MCD technique. As in the case of I_2, the parallel transition to ${}^3Q_0$ is by far the most intense. Riley and Wilson[17] studied CH_3I photodissociation at 266 nm using the technique of photofragment spectroscopy. The MCD results indicate that ${}^3Q_0$ should carry ~95% of the absorption at this wavelength. Thus, one would expect $I({}^2P_{1/2})$ to be formed almost exclusively, with a parallel polarization dependence. Riley and Wilson found that 20-25% of the I atoms are actually formed in the ground ${}^2P_{3/2}$ state. However, both the $I({}^2P_{3/2})$ and $I({}^2P_{1/2})$ products were found to be formed with a parallel polarization dependence,[17] ruling out direct contributions from the ${}^3Q_1$ and ${}^1Q_1$ states. The likely explanation of these results is that, as CH_3 and I recoil from one another along the repulsive ${}^3Q_0$ potential energy surface, there is a high probability of curve crossing to a state correlating to ground state iodine atoms (possibly the ${}^1Q_1$ state).

The first absorption continua of the higher alkyl iodides are nearly identical to that of methyl iodide, reinforcing the notion that the n -> σ^* complex of transitions is fairly characteristic of the C-I

bond. The lowest absorption continua of the alkyl bromides and alkyl chlorides are similarly broad and featureless.[13] These continua should also exhibit the characteristic structure of the Q-complex. Taking the halogens as a guide, one would expect the strength of $^3Q_0 <- N$ relative to $^1Q_1 <- N$ to decrease on going from RI to RBr to RCl. In the alkyl halides, as in the hydrogen halides, the peak of the first absorption continuum shifts to shorter wavelengths on going from I to Br to Cl. This trend reflects the stronger binding of the valence $p\pi$ electrons in the lighter halogen atoms.[18]

S.J. Lee and R. Bersohn[19] recently took a step in this direction by studying the photodissociation of methylene bromoiodide, CH_2IBr. The ultraviolet absorption spectrum of this molecule shows two broad bands: a weaker band peaking at 268 nm which is mainly due to the C-I chromophore, and a stronger band at 213 nm due to the C-Br chromophore. Lee and Bersohn used the filtered output of a high-pressure Hg-Xe arc lamp to excite a molecular beam of CH_2IBr. The excitation was broadband, extending from 235 to 345 nm. Still, most of the light was concentrated in the lower energy C-I absorption band. Under these conditions, Lee and Bersohn found that 86% of the fragmentations produced I atoms, while 14% produced Br atoms. They present additional evidence which suggests that the small yield of Br atoms results <u>not</u> from the C-I absorption band, but rather from weak residual absorption to the higher energy C-Br absorption band.

The above spectroscopic information prompted our interest in studying the photodissociation of polyatomic molecules containing two or more different carbon-halogen bonds. The $n -> \sigma^*$ transitions of the dif-

ferent carbon-halogen bonds in the molecule should still be fairly well separated in energy. Then, if the n -> σ^* transitions are truly localized on the carbon-halogen bonds, leading to prompt dissociation, it should be possible to selectively pick off one or another halogen atom from the molecule by varying the excitation wavelength.

We chose 1,2-C_2F_4BrI for our own experiments, mainly because it was commercially available. We also decided to study C_2F_5Br and C_2F_5I for comparison purposes. The substitution of fluorines for hydrogens should not change the basic molecular orbital picture described above for the alkyl halides. The non-bonding fluorine electrons can be ignored, since they are quite strongly bound (more strongly, perhaps, than some bonding electrons). The most weakly bound electrons in C_2F_4BrI will be the $5p\pi$ iodine electrons, with the $4p\pi$ bromine electrons next in line. The UV absorption spectra of C_2F_5Br, C_2F_5I and 1,2-C_2F_4BrI for $\lambda > 190$ nm are shown in Fig. 6 of Ref. 21. The first C_2F_5I absorption continuum peaks around 260 nm; C_2F_5I absorbs negligibly at 193 nm. The first C_2F_5Br continuum starts around 250 nm, and has not yet reached its maximum at 190 nm. Qualitatively, the absorption spectrum of C_2F_4BrI does indeed look like a superposition of the C_2F_5I and C_2F_5Br spectra.

In our experiments, molecular beams of C_2F_5Br, C_2F_5I and C_2F_4BrI are irradiated with pulses of UV light from a rare gas-halide excimer laser or Nd-Yag laser and photodissociation products are detected with a rotatable mass spectrometer. As expected, only C-I bond fission occurs as the primary dissociation step in C_2F_5I at 248 nm and 1,2-C_2F_4BrI at both 266 and 248 nm, and only C-Br bond fission occurs in C_2F_5Br at 193 nm. However, both C-I and C-Br bond fission are observed as primary

dissociation processes when C_2F_4BrI is irradiated at 193 nm. The laboratory angular and time-of-flight distributions of the photodissociation products are analyzed to obtain the forms of the center-of-mass recoil energy and angular distributions for these photodissociation reactions. In the case of C_2F_4BrI at 193 nm, a direct measure of the ratio of C-Br vs. C-I primary bond fission is also obtained. Some of the highly vibrationally excited C_2F_4Br and C_2F_4I produced from C_2F_4BrI at all three wavelengths are seen to undergo secondary dissociation processes.

The quantum yield measurements of Pence, Baughcum and Leone (PBL)[20] and others provide complementary information by identifying which halogen atom electronic states are produced. PBL only detected electronically excited $Br(^2P_{1/2})$ in the photodissociation of C_2F_4BrI at 193 nm; no $I(^2P_{1/12})$ emission was observed at all. The failure to detect $I(^2P_{1/2})$ was attributed to the possible selective dissociation of the C-Br bond at this wavelength. Our experimental results which will be presented in this paper are not in agreement with this conclusion. Recently, after being informed of this discrepancy, Leone and Wight[21] have carried out the quantum yield measurements again using the same experimental method. They have indeed found that the result of PBL was erroneous. Their new results give quantum yields for Br^* and I^* of 0.14 $\pm$ 0.04 and 0.50 $\pm$ 0.14, respectively.

II. EXPERIMENTAL DETAILS

A) Photodissociation of C_2F_5I, C_2F_5Br and C_2F_4BrI at 248 and 193 nm.

The molecular beams were formed by expanding Ar-seeded mixtures of the sample gases through a 0.12 mm diameter hole at the end of a stainless steel nozzle. The nozzle tip was heated to 240°C to inhibit cluster formation in the supersonic expansion. The C_2F_5Br, C_2F_5I and 1,2-C_2F_4BrI samples were purchased from PCR Research Chemicals, Inc. Ten percent mixtures of C_2F_5Br and C_2F_5I in Ar were prepared ahead of time in mixing tanks. In the case of 1,2-C_2F_4BrI, the liquid sample was held in a temperature controlled reservoir maintained at -10°C (C_2F_4BrI partial pressure ≈ 22 torr), and Ar carrier gas was bubbled through the liquid to give a total stagnation pressure of 300 torr. The C_2F_5Br/Ar and C_2F_5I/Ar mixtures were also run at a stagnation pressure of 300 torr.

As usual, the beam source utilized three stages of differential pumping. The first skimmer (1.15 mm diameter), mounted on the source reducer, defined the molecular beam to an angular divergence of ~10.5°. A second skimmer-like aperture (1.2 mm diameter), mounted on the middle wall of the differential pumping chamber, defined the molecular beam to a final angular divergence of 1.6°. A 4 mm x 4 mm square slit, mounted at the front of the third and final differential pumping region, was large enough to let the molecular beam pass cleanly through and into the main interaction chamber, where it was crossed at right angles by the laser beam. (The square slit served only to reduce the amount of effusive background entering the detector at small viewing angles). The total distance from the nozzle to the crossing point of the laser and

molecular beams was 10.0 cm.

Beam velocity distributions were determined by conventional time-of-flight (TOF) measurements. For each gas mixture, two beam calibrations were performed. The data were fit to the usual assumed form for the beam number density velocity distribution, $N(v) \propto v^2 \exp[-(\frac{v}{\alpha} - S)^2]$, The best-fit parameters are listed in Table 1. For each gas, the values obtained for the peak molecular beam velocity from the two calibrations agree within ~1%. The deviations in the individual parameters α and S are larger, reflecting the lower sensitivity of the calibration method and/or the fitting procedure to the width of the velocity distribution. For no particular reason, the α and S values from calibration #1 were actually used to reproduce the beam velocity distribution in the data fitting to be described in Sec. III.

The source of UV radiation was a Lambda Physik EMG 101 excimer laser. The laser was run at a repetition rate of 30 Hz. We obtained average laser pulse energies of 100-130 mJ/pulse on the KrF excimer transition at 248 nm and 5-25 mJ/pulse on the ArF excimer transition at 193 nm. The unpolarized, rectangular-shaped laser beam was focussed to a 4 mm^2 spot at the point where it crossed the molecular beam by a 35 cm focal length, UV-grade fused silica lens. This resulted in a (time-integrated) photon flux of $\Phi = 3 - 4 \cdot 10^{18}$ photons/cm^2-pulse and laser intensities of I = 160-200 MW/cm^2 at 248 nm, and $\Phi = 1.2 - 6 \cdot 10^{17}$ photons/cm^2-pulse, I = 9-45 MW/cm^2 at 193 nm (assuming pulse durations of 16 ns at 248 nm and 14 ns at 193 nm, as quoted by Lambda Physik).

Photodissociation products were detected in the plane of the laser and molecular beams by a rotatable ultra-high vacuum mass spectrometer

consisting of an ionizer, a quadrupole mass filter, and a Daly-type ion counter. The new ionizer utilizes a permanent ceramic magnet to confine a longitudinal electron beam along the axis of the detector. This design offers comparable sensitivity to the conventional Brink ionizer for "beam" molecules (which pass through the defining slits of the detector), with reduced sensitivity to background molecules and improved spatial resolution (due to a smaller effective ionization volume). The distance from the interaction region to the center of the ionizer is 20.8 cm. Product TOF distributions were obtained by multiscaling the mass spectrometer output following a laser pulse using a 255-channel multiscaler. The scaler was triggered by a reference pulse from the excimer laser. The offset between the reference pulse and the laser pulse was checked and found to be negligible (~200 ns). Laboratory angular distributions were usually obtained by integrating and normalizing the TOF distributions measured at several detector angles.

In the case of C_2F_5Br at 193 nm, the only data recorded was a Br^+ TOF distribution at a laboratory angle of 10°. The Br^+ signal level was ~0.02 counts/pulse for laser pulse energies of 5-15 mJ. The TOF distribution was integrated over $2 \cdot 10^5$ laser pulses. At 248 nm, with 100 mJ laser pulse energies, no Br^+ signal could be detected ($\leq$0.006 counts/pulse at the 1σ confidence level).

For C_2F_5I at 248 nm, signal was observed at m/e = 127, 119, 100, 69, 50 and 31, corresponding to I^+, $C_2F_5{}^+$, $C_2F_4{}^+$, $CF_3{}^+$, $CF_2{}^+$ and CF^+. TOF distributions of I^+ and $C_2F_4{}^+$ were measured at four detector angles (10°, 20°, 30° and 40° from the molecular beam). These TOF distributions were summed over 20,000-50,000 laser pulses at each angle. TOF

distributions at the other ion masses were measured only at 10°. The I^+ and $C_2F_4^+$ signal levels at 10° were 1.7 and 0.5 counts/pulse, respectively, for 130 mJ KrF pulse energies. At 193 nm, with 15 mJ ArF pulse energies, no $C_2F_4^+$ or I^+ signal could be detected ($\lesssim$0.01 counts/pulse).

For C_2F_4BrI at 248 nm, signal was observed at m/e = 127, 100, 81, 79, and 50, corresponding to I^+, $C_2F_4^+$, ($^{81}Br^+/C_2F_3^+$), $^{79}Br^+$ and CF_2^+. Signal was probably also present at CF_3^+ and CF^+ but these ions were not monitored. No significant $C_2F_4Br^+$, CF_2Br^+ or $CFBr^+$ signal could be detected ($\lesssim$0.02 counts/pulse). TOF distributions of I^+ were measured at four detector angles (10°, 20°, 30°, 40°), summing over 20,000 -30,000 laser pulses at each angle. TOF distributions at the other ion masses were measured only at 10°. The laboratory angular distribution of the I^+ signal was also measured between 8° and 41°, in 3° increments, by gating a dual-channel scaler in the usual way. Three scans were made, with a total of 6000 laser pulses at each angle. The actual I^+ and $C_2F_4^+$ signal levels at 10° were 1.1 and 0.3 counts/pulse, respectively, for 100 mJ KrF pulse energies. At 193 nm, only I^+ and Br^+ were monitored. (The quadrupole resolution was set low enough to collect both Br isotopes). TOF distributions of both I^+ and Br^+ were measured at four detector angles (10°, 20°, 30°, 40°). Because of the large fluctuations and rapid drifts in the laser power at 193 nm, these TOF measurements were made in a staggered fashion. In both cases, five scans were made, accumulating signal for 5000 laser pulses per angle per scan, and reversing directions between scans (i.e., 10° -> 40°, 40° -> 10°, . . .). Therefore, even with the large power fluctuations, the relative I^+ and Br^+ signal intensities measured at the four detector angles should be

correct. The I^+ and Br^+ signal levels at 10° were 0.4 and 0.2 counts/pulse, respectively, for 25 mJ ArF pulse energies.

B) Photodissociation of C_2F_4BrI at 266 nm.

The 266 nm experiments were performed two years later in order to better answer some of the questions raised in the photodissociation of C_2F_4BrI at 248 nm. The setup was as described above with the following exceptions. The C_2F_4BrI/Ar beam was formed as above but expanded through a nozzle heated to 190°C. The first skimmer was .38 mm in diameter and defined the beam to a 3.9° angular divergence. The second skimmer was 1.0 mm in diameter and defined the beam to final angular divergence of 2.1°. The 4 mm x 4 mm slit was left as it was in the preceding experiments. The total distance from the nozzle to the crossing point of the laser and molecular beam was 9.45 cm.

The beam velocity distribution was measured at the beginning of the experiment by a conventional TOF technique and crudely during the experiment by measuring the shape of signal depletion from the beam caused by the laser firing at the interaction region and the subsequent spreading of the hole by the time that portion of the beam reached the detector. Both sets of parameters are given in Table 1. The values obtained for the peak molecular beam velocity from the two different calibration procedures agreed to within ~1%. The conventional measurement results were used in the data analysis as better statistics were obtained.

The pulsed source of 266 nm radiation was a Quanta-Ray Nd:Yag laser operating at a repetition rate of 10 Hz. The average laser pulse energy was 35 mJ/pulse. The laser beam was polarized in the direction of the molecular beam velocity and focused to a 2.8 mm diameter doughnut shaped

spot at the crossing point with the molecular beam with a 50 cm focal length spherical fused silica lens. This resulted in a time-integrated photon flux of 7.6×10^{17} photons/cm^2·pulse.

The photodissociation products were detected in the plane of the laser and molecular beam with the same detector previously described but with different voltages on the electron and ion lenses in the ionizer which resulted in a slightly longer flight path of 21.2 cm.

At 266 nm, data was collected at m/e = 127, 100, 79, and 50 corresponding to I^+, $C_2F_4^+$, $^{79}Br^+$, and CF_2^+. TOF distributions of I^+ were measured at four detector angles (10°, 20°, 30°, and 40°) summing over 110,000 laser shots at 10° to 290,000 laser shots at 40°. TOF distributions at the other masses were measured only at 10°. A crude laboratory angular distribution of the I^+ signal was obtained at the four angles above by integrating the portions of the TOF data for which the laser power was kept constant. The average signal in 40,000 laser shots was computed from 2 to 4 scans of 40,000 laser shots at each angle. The actual I^+ and C_2F_4 signal levels at 10° were .056 and .033 counts/laser pulse respectively for the ~35 mJ/pulse laser energy.

III. RESULTS AND ANALYSIS

The primary photodissociation reactions studied here are:

$$(1)\quad C_2F_5Br \xrightarrow{193\ nm} C_2F_5 + Br$$

$$(2)\quad C_2F_5I \xrightarrow{248\ nm} C_2F_5 + I$$

$$(3a)\quad C_2F_4BrI \xrightarrow{248\ nm} C_2F_4Br + I$$

$$(3b)\quad \xrightarrow{266\ nm} C_2F_4Br + I$$

$$(4a)\quad C_2F_4BrI \xrightarrow{193\ nm} C_2F_4Br + I$$

$$(4b)\quad \xrightarrow{193\ nm} C_2F_4I + Br$$

Our primary experimental data consists of the laboratory TOF distributions, $N(t)$, and laboratory angular distributions, $N(\Theta)$, of the atomic (I or Br) products. Since large amounts of energy are involved in these photodissociation reactions, the polyatomic products are not always stable. Therefore, we mainly rely on the atomic products to tell us about the primary photodissociation dynamics. The goal of the data analysis is to extract the forms of the center-of-mass (c.m.) product translational energy distribution, $P(E_T)$, and angular distribution, $w(\Theta)$, from the measured $N(t)$'s and $N(\Theta)$.

For a single photon absorption process in the electric dipole approximation, the c.m. angular distribution must have the form[22]

$$w(\theta) = \frac{1}{4\pi}\,[1 + \beta P_2(\cos\theta)],$$

where θ is the angle between the electric vector of the laser light and the final (c.m.) recoil direction of the products, and where the aniso-

tropy parameter, β, is constrained to lie in the range $-1 \leq \beta \leq 2$. If dissociation occurs in a time short compared to a rotational period, and if averaging effects due to the finite amplitudes of the bending vibrations are ignored, then the anisotropy parameter is related to the angle, α, between the transition dipole moment and the bond dissociation coordinate according to [23]

$$\beta = 2\, P_2(\cos\alpha).$$

For a pure parallel transition, $\alpha = 0°$, $\beta = +2$, and $w(\theta)$ reduces to a $\cos^2\theta$ angular distribution. For a pure perpendicular transition, $\alpha = 90°$, $\beta = -1$, and $w(\theta)$ reduces to a $\sin^2\theta$ angular distribution.

As usual, a trial-and-error (forward convolution) fitting procedure is used. The shape of the $P(E_T)$ and a value of are guessed. This allows the angle-velocity flux distribution of the detected fragment to be calculated in the c.m. reference frame. The usual c.m. -> LAB transformation is made (taking into account averaging over the molecular beam velocity distribution and the finite size of the ionizer and interaction volume), yielding the laboratory velocity flux distribution of the detected fragment at various detector angles. These velocity flux distributions are converted to number density vs. time distributions and compared to the measured N(t) distributions. The calculated N(t) distributions are also integrated to give a calculated $N(\Theta)$ distribution which can be compared to the experimental angular distribution. The value of β and the shape of the $P(E_T)$ are varied, and the calculation repeated, until a good simultaneous fit to all of the experimental data is obtained.

In these experiments, the c.m. recoil velocities of the products tend to be substantially larger than the molecular beam velocities. At a given laboratory angle, only a rather small range of c.m. angles are sampled. Therefore, the shapes of the calculated N(t) distributions are mainly sensitive to the $P(E_T)$, while the shape of the calculated $N(\Theta)$ distribution is mainly sensitive to β. (Of course, in the limit that the product recoil velocity is very large compared to the molecular beam velocity, we would actually be doing the experiment in the c.m. reference frame.) This decoupling of the laboratory angular and TOF distributions makes the data fitting very easy, since the shape of the $P(E_T)$ and the value of β can be optimized almost independently.

For all of the reactions studied here, the halogen atoms may be formed in either the ground $^2P_{3/2}$ state or the spin-orbit excited $^2P_{1/2}$ state. (From now on, we will denote $I(^2P_{1/2})$ and $Br(^2P_{1/2})$ by I^* and Br^*). The fine-structure splitting is 21.7 kcal/mole in iodine, 10.54 kcal/mole in bromine. Our experiments do not reveal directly which halogen atom states are produced. However, in no case do we observe evidence of bimodality in the derived product translational energy distribution. This suggests (but does not prove) that only one fine-structure state is formed in each reaction.

Due to the interest in atomic photodissociation lasers, a number of experiments have been performed to determine the quantum yields for I^* and Br^* formation from the alkyl iodides and alkyl bromides.[21,24-27,39] These experiments indicate that I^* should be formed almost exclusively in reactions (2) and (3). We will assume that this is true in the analysis below. Unfortunately, the evidence is not so clear-cut in the

case of reactions (1), (4a) and (4b); we will not make a judgment in this section as to which halogen atom electronic state predominates in these reactions. In Sec. IV, the quantum yield measurements and the problem of identifying the product electronic states will be discussed in some detail.

We will present and analyze our results on C_2F_5Br, C_2F_5I and 1,2-C_2F_4BrI in parts A, B and C below. Whenever experimental angular distributions are displayed, the error bars represent plus and minus two standard deviations of the statistical counting error. When TOF distributions are displayed, the time scale always includes the flight time of the ions through the mass spectrometer. For the magnetic ionizer, under our operating conditions, the ion flight time in $s = 1.8\sqrt{M}$, where M is the ion mass in amu's. To convert to lab velocities, the displayed flight times must be corrected for the ion flight time and divided into the nominal product flight distance of 20.8 cm. Finally, we should mention that the experimental and calculated TOF distributions have always been normalized to the same peak height at each angle, thereby allowing the shapes of the calculated TOF distributions to be compared to the data independently of differences in the calculated and experimental angular distributions.

A. C_2F_5Br

As mentioned in Sec. II, the only data we took on C_2F_5Br was a Br^+ TOF distribution at 10° from the molecular beam.[28] This is shown in Fig. 1. This lone TOF distribution is almost completely insensitive to the value of the anisotropy parameter for reaction (1). The solid curve in Fig. 1 was calculated from a simple trapezoidal-shaped $P(E_T)$ with a mean

translational energy of 30 kcal/mole and a FWHM energy spread of 11 kcal/mole. Due to the poor quality of the data we did not attempt to do anything fancy with the $P(E_T)$. For concreteness, the value $\beta = +2$ was used in the calculation. This value for the anisotropy parameter was chosen only because values close to two were found for all of the other photodissociation reactions studied here (see below).

The photon energy at 193.3 nm corresponds to 147.8 kcal/mole. The C_2F_5-Br bond strength is 68.6 kcal/mole.[28] If ground state Br atoms are formed exclusively, then 79 kcal/mole remains to be partitioned between product translation and the internal (vibrational + rotational) degrees of freedom of C_2F_5. The most probable dissociation event channels ~30 kcal/mole into product translation, leaving 49 kcal/mole in the C_2F_5 radical. However, the width of the product translational energy distribution implies that some dissociation events produce C_2F_5 + Br products with recoil energies as low as 21 kcal/mole. This would leave as much as 58 kcal/mole of internal energy in the C_2F_5. The C-C bond strength in C_2F_5 is approximately 56 kcal/mole:[30]

(5) $C_2F_5 \longrightarrow CF_3 + CF_2 \quad \Delta H = 56$ kcal/mole.

Therefore, if ground state Br atoms are formed, it is possible that some of the hottest C_2F_5 primary products spontaneously decompose to CF_3 + CF_2. If, on the other hand, Br^* atoms are formed, no spontaneous C_2F_5 decay would be possible. Measurements of TOF distributions at other ion masses ($C_2F_4^+$, CF_3^+, CF_2^+) would reveal whether or not reaction (5) is actually occurring.

B. C_2F_5I

The I^+ TOF distributions measured at 248 nm are displayed in Fig. 2. These distributions were integrated and normalized to give the laboratory angular distribution of I^+ in Fig. 3. The solid curves in Figs. 2 and 3 were calculated using the $P(E_T)$ shown in Fig. 4 and β = 1.87. This $P(E_T)$ has a mean translational energy of 20.9 kcal/mole and a FWHM energy spread of 6.8 kcal/mole. The dashed curves in Fig. 3 were calculated using the same $P(E_T)$ but different values of β, to illustrate the sensitivity of the laboratory angular distribution to the anisotropy parameter. The derived value of β is very close to the value β = 2 expected for a pure parallel transition (transition dipole moment oriented parallel to the C-I bond).

As mentioned earlier, there is good reason to believe that all of our I^+ signal at 248 nm is due to excited I^* atoms. The photon energy at 248.4 nm corresponds to 115.0 kcal/mole. Subtracting the C_2F_5-I bond dissociation energy of 52.5 kcal/mole[31] and the I^* electronic energy of 21.7 kcal/mole leaves 41 kcal/mole to be distributed between product translational energy and C_2F_5 internal energy. The average recoil energy of 20.9 kcal/mole corresponds to 51% of this available energy. Thus, on the average, the C_2F_5 radicals should be formed with 20 kcal/mole internal energy, which is well below the C_2F_5 dissociation threshold. No spontaneous decay of C_2F_5 should be possible in this case.

The laboratory TOF and angular distributions of C_2F_5 shown in Figs. 5 and 6 confirm this expectation. For these measurements, C_2F_5 was monitored as $C_2F_4^+$ in the mass spectrometer. The $P(E_T)$ and β value that were used to fit the I^+ data also provide an excellent fit to the $C_2F_4^+$

data. None of the C_2F_5 radicals have "disappeared." Comparing the $C_2F_4^+$ and I^+ angular and TOF distributions, one sees that, at each angle, the $C_2F_4^+$ product is slightly faster than the I^+ product (even after correcting for the small difference in ion flight times), and that the $C_2F_4^+$ angular distribution is a little broader than that of I^+. This reflects the requirement imposed by conservation of linear momentum. The effect is quite small, since C_2F_5 (m = 119) is only slightly lighter than I (m = 127).

TOF distributions of $C_2F_5^+$, CF_3^+, CF_2^+ and CF^+, measured at 10°, were superimposable on the $C_2F_4^+$ TOF distribution (after corrections for ion flight time were made). This confirms that all of these ions arise from C_2F_5 radicals and that no secondary dissociation processes are occurring.

C. 1,2-C_2F_4BrI

1. 248 nm

At 248 nm, the only primary dissociation channel observed is C-I bond fission. The measured I^+ TOF and angular distributions are shown in Figs. 7 and 8, respectively. The four open circles in Fig. 8 were obtained by integrating and normalizing the I^+ TOF distributions in Fig. 7. The solid circles represent the average of the three angular scans performed using the dual-channel scaler. The solid curves in Figs. 7 and 8 were calculated using $\beta = 1.84$ and the $P(E_T)$ shown in Fig. 9. This $P(E_T)$ has a mean translational energy of 19.5 kcal/mole and a FWHM of 11.1 kcal/mole. The two dashed curves in Fig. 8 were calculated using the same $P(E_T)$ but slightly different values of β.

Except for the fact that the $P(E_T)$ is significantly broader in this case, these results are very similar to the corresponding results for C_2F_5I. Again we will assume that all of our I^+ signal at 248 nm is due to I^*. If the C-I bond strength is the same in C_2F_4BrI as in C_2F_5I, then 41 kcal/mole is available for product translation and C_2F_4Br internal excitation. The mean translational energy of 19.5 kcal/mole represents 48% of this available energy, leaving 21.5 kcal/mole, on the average, in the C_2F_4Br radicals.

C_2F_4Br, unlike C_2F_5, has a very low energy dissociation channel. Using available thermochemical data we estimate that the C_2F_4-Br bond strength is only 16 kcal/mole:[33]

(6) $C_2F_4Br \longrightarrow C_2F_4 + Br \quad \Delta H = 16$ kcal/mole.

We will assume that the threshold energy for reaction (6) is not much greater than the endothermicity.[34] Then most, if not all, of the C_2F_4Br formed in reaction (3) should spontaneously decompose to C_2F_4 + Br. The TOF distributions of $C_2F_4^+$ and $^{79}Br^+$ shown in Fig. 10 support this expectation. (Ignore for a moment the sharp "spike" on the $C_2F_4^+$ distribution at ~175 μs.) The broad $C_2F_4^+$ and $^{79}Br^+$ signals are assigned to the C_2F_4 and Br products of the spontaneous dissociation reaction (6). The extra translational energy released in the secondary reaction causes the C_2F_4 and Br products to be smeared out in the laboratory. Note that the $^{79}Br^+$ TOF distribution is somewhat faster and broader than that of $C_2F_4^+$, as expected on the basis of the kinematics of reaction (6). The TOF distribution measured at m/e = 81 (not shown) was intermediate in width between the $C_2F_4^+$ and $^{79}Br^+$ distributions. The signal at m/e = 81 was twice that at m/e = 79. Since the isotopic abundances

of ^{79}Br and ^{81}Br are nearly equal, half of the m/e = 81 signal must be due to $C_2F_3^+$. By subtracting the m/e = 79 TOF distribution from the m/e = 81 distribution, we obtained the form of the $C_2F_3^+$ TOF distribution. The latter agreed very well with the $C_2F_4^+$ TOF distribution, <u>except that the spike appeared to be absent in the $C_2F_3^+$ distribution</u>.

What is the origin of the spike on the $C_2F_4^+$ TOF distribution, and why does it appear only at $C_2F_4^+$? Evidently, the spike is due to stable C_2F_4Br radicals which are formed in the primary dissociation reaction (3a) with lower than average internal energies. We noted above that the mean product recoil energy of 19.5 kcal/mole corresponds to a C_2F_4Br internal energy of 21.5 kcal/mole, which is ~6 kcal/mole greater than the C_2F_4-Br bond dissociation energy. All primary dissociation events giving product recoil energies greater than 25 kcal/mole should produce C_2F_4Br radicals with less than 16 kcal/mole internal energy, and these should survive. According to Fig. 9, around 10% of the primary dissociation events fall into this category.

The position and width of the spike in the $C_2F_4^+$ TOF distribution are consistent with the above interpretation. The arrow in Fig. 10 indicates the most probable flight time at which C_2F_4Br would appear in the $C_2F_4^+$ TOF distribution <u>if none of the C_2F_4Br radicals spontaneously decomposed.</u> That is, the position of the arrow was calculated using the mean C_2F_4Br + I recoil energy of 19.5 kcal/mole from Fig. 9. The observed spike is definitely skewed towards shorter flight times, indicating that, in fact, only the faster C_2F_4Br radicals with lower internal energies survive. It is interesting to note that, if ground state I atoms were formed in reaction (3a), it would be impossible for any of

the C_2F_4Br radicals to survive. Thus, our observation of C_2F_4Br supports the conclusion from the quantum yield measurements that I^* is formed in this reaction.

It is a bit surprising that the surviving C_2F_4Br does not make its presence felt at other ion masses. No significant $C_2F_4Br^+$, CF_2Br^+ or $CFBr^+$ was detected, and there was no noticeable spike on the measured CF_2^+ or derived $C_2F_3^+$ TOF distributions. The ion $C_2F_4^+$ evidently dominates the mass spectrum of the C_2F_4Br radical. Of course, there really isn't much C_2F_4Br signal in the $C_2F_4^+$ spike, either (~0.01 counts/pulse).

2. 266 nm

The only primary photochemical step observed in the photodissociation of C_2F_4BrI at 266 nm was cleavage of the C-I bond. In addition to deriving c.m. product translational energy and angular distributions, we were also able to conclude from a comparison of I^+ and $C_2F_4{}^+$ TOF data that almost every dissociation gives excited state I^* product and to extract an approximate value for the dissociation energy of C_2F_4Br to C_2F_4 + Br.

The m/e = 127, I^+, TOF data taken at detector angles of 10°, 20°, 30°, and 40° from the molecular beam are shown in Fig. 11. The corresponding laboratory angular distribution of the I^+ signal is shown in Fig. 12. A simultaneous fit to the TOF data and angular distribution gave the $P(E_T)$ shown in Fig. 13 for the primary process (3b) and an approximate anisotropy parameter of $\beta = 1.8$.

The identification of the majority of the I atom produced in reaction (7) as being electronically excited can be made from a comparison of the $C_2F_4^+$ and I^+ TOF data. The TOF of m/e = 100, $C_2F_4^+$, is shown in Fig. 14. Signal at $C_2F_4^+$ can originate from two sources as explained in the 248 nm section, from C_2F_4Br radicals and from C_2F_4 molecules produced from the secondary dissociation of the vibrationally hot C_2F_4Br radicals. The sharp spike in the $C_2F_4^+$ TOF distribution is the C_2F_4Br signal while the broad underlying background is the C_2F_4 signal. One easily calculates that the observed C_2F_4Br signal matches the faster I atom product by momentum conservation; this is seen in the $P(E_T)$ shown in dotted line in Fig. 13 which fit the C_2F_4Br signal in the $C_2F_4^+$ TOF. The fact that the fastest C_2F_4Br radicals survive (do not undergo secondary dissociation) immediately suggests that there is little or no ground state I produced in the primary reaction. If ground state I atoms were formed, they would be detected on the faster side of the TOF distribution as there would be approximately 10 more kilocalories of recoil energy (see Ref. 17). However, the C_2F_4Br radical that would be formed with the ground state I atom could not survive; even after channeling the maximum observed 30 kcal/mole of energy to translation the C_2F_4Br fragment would still have more than 25 kcal/mole of internal energy and would dissociate to C_2F_4 + Br. Thus, the C_2F_4Br spike could not match the fast part of the I^+ atom TOF distribution if a significant fraction of the dissociations produced ground state iodine. In addition, the similarity between this $P(E_T)$ and the $P(E_T)$ at 248 nm supports the conclusion that only spin-orbit excited iodine is formed at that wavelength.

One may also extract an approximate value for the barrier to dissociation of C_2F_4Br to C_2F_4 + Br from a comparison of the translational energy distributions, Fig. 13, derived from the I^+ and $C_2F_4^+$ TOF data. Fig. 13 shows that C_2F_4Br radicals begin to survive only when the relative translational energy of the C_2F_4Br + I* products of the primary dissociation reaction is $\geq$ 14 kcal/mole. The C_2F_4Br produced at lower translational energies appears to have all dissociated. Assuming there is no barrier to the dissociation of C_2F_4Br beyond the endothermicity, one then obtains the dissociation energy of the C_2F_4Br radical from energy conservation:

$$D_o(C_2F_4\text{-}Br) = E_{h\nu} - D_o(C_2F_4Br\text{-}I) - E_{elec}(I^*) - E_T$$

$$= 107.5 - 52.5 - 21.7 - 14.0$$

$$= 19.3 \text{ kcal/mole}$$

Note that this value is quite close to the value estimated in footnote 33 using available thermochemical data. The C_2F_4Br radicals that survive at a recoil energy of 14 kcal/mole have been formed from parent molecules with the least internal energy. The average internal energy of the parent at 190°C is only 7 kcal/mole before the expansion, so a significant fraction of the parent molecules should be in the ground vibrational state, particularly after the expansion. Even assuming no relaxation in the expansion, almost 5% of the parent molecules have less than half a kcal of vibrational energy. It will be C_2F_4Br radicals from these parent molecules that will survive at the threshold translational energy. Thus we have not included a parent internal energy in the expression above. One might also be concerned that although a given

C_2F_4Br product has enough energy to dissociate, it may not do so within the 200 sec flight time to the detector. However, we estimate the dissociation lifetime of C_2F_4Br radicals with only .2 kcal/mole of energy above a 16 kcal/mole dissociation limit to be less than a microsceond. (This is calculated from RRKM theory assuming an A-factor of 15.) Thus the barrier for dissociation of C_2F_4Br to C_2F_4 + Br is found to be 19.3 kcal/mole. This uncertainty lies mainly in the uncertainty of which of the $C_2F_4^+$ signal to attribute to C_2F_4Br on the slow side of the sharp feature in Fig. 14. This value of 19.3 kcal/mole for the barrier is also dependent upon our assumption that the C-I bond dissociation energy is 52.5 kcal/mole.

3. 193 nm

C-I and C-Br bond fission compete at 193 nm. I^+ and Br^+ TOF distributions were measured at four detector angles. The distributions measured at 10 are shown in Fig. 15. As noted on the figure, the sharp features are assigned to the I and Br atoms formed in the primary photodissociation reactions (4a) and (4b), while the broad underlying signals result when the hot C_2F_4I and C_2F_4Br primary products undergo spontaneous unimolecular decay to C_2F_4 + I and C_2F_4 + Br, respectively. We will show below that, at this short wavelength, none of the C_2F_4I or C_2F_4Br primary products can survive regardless of which halogen atom electronic states are formed.

The relative intensities of the primary iodine and bromine atom signals as a function of laboratory angle were obtained by integrating the sharp peaks in the I^+ and Br^+ TOF distributions. The results are listed in Table 2. In the case of iodine, the signal at each angle was

integrated between 120-180 μs. In the case of bromine, the signal was integrated between 90-140 μs. Obviously, the presence of the underlying secondary dissociation signal in the I^+ and Br^+ TOF distributions creates some ambiguity in the above determinations. However, for both I^+ and Br^+, the broad secondary signal and the sharp primary signal were found to fall off at about the same rate as the laboratory angle was increased. Therefore, the experimental numbers in Table 2 should be fairly reliable.

We used the laboratory angular and TOF distributions of the primary iodine and bromine atom signals to determine the shapes of the c.m. translational energy and angular distributions for reactions (4a) and (4b). First consider reaction (4a). The solid curve in the top panel of Fig. 11 was calculated using a symmetric, triangular-shaped $P(E_T)$ with a mean translational energy of 27.0 kcal/mole and a FWHM energy spread of 13.0 kcal/mole. The value $\beta = 1.85$ gives the best fit to the laboratory angular distribution of iodine (see Table 2). We conclude that: (i) when C_2F_4BrI is irradiated at 193 nm, C_2F_4Br + I products are formed; (ii) the combined c.m. recoil energy of the C_2F_4Br + I products is, on the average, 27.0 kcal/mole; (iii) the electronic transition leading to formation of these products is polarized parallel to the C-I bond. If ground state iodine atoms are formed in reaction (4a), then the energy available to the C_2F_4Br + I products is approximately 95 kcal/mole. Subtracting the mean recoil energy of 27 kcal/mole leaves, on the average, 68 kcal/mole in the C_2F_4Br. If instead I^* atoms are formed, the mean C_2F_4Br internal energy is reduced to 47 kcal/mole, but this is still far above the C_2F_4-Br bond dissociation energy. There-

fore, in either case, all of the C_2F_4Br radicals will spontaneously decompose to C_2F_4 + Br.

We now turn to reaction (4b). The solid curve in the bottom panel of Fig. 11 was calculated using a symmetric, triangular-shaped $P(E_T)$ with a mean translational energy of 25.5 kcal/mole and a FWHM of 9.0 kcal/mole. A value of β between 1.70 and 1.85 gives the best fit to the bromine atom angular distribution (Table 2). We conclude that: (i) when C_2F_4BrI is irradiated at 193 nm, C_2F_4I + Br products are formed; (ii) the combined c.m. recoil energy of the C_2F_4I + Br products is, on the average, 25.5 kcal/mole; (iii) the electronic transition leading to formation of these products is polarized parallel to the C-Br bond. We will assume that the C-Br bond strength in C_2F_4BrI is the same as in C_2F_5Br (69 kcal/mole). Then, if ground state Br atoms are formed in reaction (4b), there is 79 kcal/mole available to the C_2F_4I + Br products. Subtracting the observed mean translational energy of 25.5 kcal/mole leaves around 54 kcal/mole in the C_2F_4I product. If Br^* is produced, the mean C_2F_4I internal energy is 10.5 kcal/mole less. Since the C-I bond in C_2F_4I is extremely weak,[33]

(7) $C_2F_4I \longrightarrow C_2F_4 + I \quad \Delta H \approx 0$ kcal/mole,

all of the C_2F_4I primary products will spontaneously decompose regardless of which Br electronic state is formed.

We now wish to determine the absolute ratio, R, of C-I vs. C-Br bond fission at 193 nm. The determination of R involves the usual two steps.[35] First, the measured $I^+:Br^+$ ion signal ratio must be corrected to give the true laboratory I:Br signal ratio at a given laboratory angle. And second, this lab signal ratio must be transformed to the

c.m. system. At 10°, the actual I^+ and Br^+ signal levels (considering only the sharp peaks in the TOF distributions) were 0.31 counts/pulse and 0.10 counts/pulse, respectively. Thus,

$$\frac{N_{I^+}(10°)}{N_{Br^+}(10°)} = 3.1.$$

This ion signal ratio is related to the true laboratory I:Br product ratio according to

$$\frac{N_{I^+}(10°)}{N_{Br^+}(10°)} = \frac{N_I(10°)}{N_{Br}(10°)} \cdot \frac{\sigma_{ion}(I)}{\sigma_{ion}(Br)} .$$

$\sigma_{ion}(I)$ and $\sigma_{ion}(Br)$ are the ionization cross sections of I and Br. The ionization cross sections (in $Å^2$) may be estimated semi-empirically using the relation[36]

$$\sigma_{ion} = 36\sqrt{\alpha} - 18 ,$$

where α is the species polarizability in $Å^3$. From Ref. 36, we have $\alpha(I) = 3.9$, $\alpha(Br) = 3.05$; therefore $\sigma_{ion}(I) = 53.1$, $\sigma_{ion}(Br) = 44.9$, and

$$\frac{N_I(10°)}{N_{Br}(10°)} = (3.1) \cdot \left(\frac{44.9}{53.1}\right)$$

$$= 2.6.$$

Using the best-fit c.m. translational energy and angular distributions for reactions (4a) and (4b), described earlier, we calculated the laboratory I:Br product ratio at 10° as a function of R. We obtained

$$\frac{N_I(10°)}{N_{Br}(10°)} = 1.533 \cdot R.$$

Thus, R = 2.6/1.533 = 1.7; at 193 nm, C-I bond fission dominates C-Br bond fission by almost two to one.

IV. DISCUSSION

Mulliken concluded that: (i) the lowest UV absorption continua in the alkyl halide molecules are due to transitions of non-bonding halogen electrons to anti-bonding σ^* molecular orbitals on the adjacent carbon-halogen (C-X) bonds; (ii) each n -> σ^* absorption continuum should contain transitions to three excited states, $^3Q_1$, $^3Q_0$, and $^1Q_1$; (iii) the transition to $^3Q_0$ should be polarized parallel to the C-X bond and correlate to X^* product, while the transitions to $^3Q_1$ and $^1Q_1$ should be polarized perpendicular to the C-X bond and correlate to ground state X product. Mulliken argued that the n -> σ^* transition complex, or "Q-complex," is a characteristic feature of each carbon-halogen bond. The fact that the peak of the n -> σ^* absorption continuum shifts to shorter wavelengths on going from the alkyl iodides to the alkyl bromides to the alkyl chlorides suggested the interesting possibility of doing bond-selective (BS) photochemistry in molecules containing two or more different carbon-halogen bonds.

The present experiments on C_2F_5Br, C_2F_5I, and 1,2-C_2F_4BrI were intended to explore this possibility. The "control" molecules, C_2F_5Br and C_2F_5I, behaved as expected: only C-I bond fission was observed in C_2F_5I at 248 nm, and only C-Br bond fission was observed in C_2F_5Br at 193 nm. We anticipated that C_2F_4BrI would behave like C_2F_5I at 248 nm, and like C_2F_5Br at 193 nm. In fact, only C-I bond fission was observed at 248 nm. However, at 193 nm, both C-Br and C-I bond fission were observed, with a C-I:C-Br fission ratio of 1.7:1.

All of these photodissociation reactions will be discussed in detail below. The C-I fission reactions of C_2F_5I and C_2F_4BrI at 248 nm

will be discussed together in part A, since they are similar and reasonably well-understood. The C-Br fission reaction of C_2F_5Br at 193 nm will be considered briefly in part B. Finally, in part C, we will return to the more complicated behavior of C_2F_4BrI at 193 nm, and discuss possible reasons for the observed competition between C-Br and C-I bond fission.

A. C_2F_5I at 248 nm and 1,2-C_2F_4BrI at 248 nm and 266 nm

The alkyl and perfluoroalkyl iodides have been extensively studied in connection with their use in atomic iodine photodissociation lasers. Donohue and Wiesenfeld[24] used time-resolved atomic absorption spectroscopy to measure the quantum yields for I^* formation following broad-band photolysis of a number of alkyl and perfluoroalkyl iodides. They obtained I^* quantum yields greater than 90% for each of CF_3I, C_2F_5I, n-C_3F_7I, and i-C_3F_7I. In the case of C_2F_5I and n-C_3F_7I, the broad-band I^* quantum yields were especially high, > 98% and > 99%, respectively.

These broad-band measurements only reveal the average value of the I^* quantum yield over the entire n -> σ^* absorption continuum. In principle, the I^* quantum yield may vary as a function of wavelength, due to the underlying structure of the Q-complex. However, the wavelength-specific measurements of Koffend and Leone[27] indicate that, in the case of n-C_3F_7I, the I^* quantum yield is essentially flat between 265 and 340 nm. Wavelength-specific quantum yields for C_2F_5I and 1,2-C_2F_4BrI have been determined at 248[39], 268[21] and 308[39] nm for C_2F_5I and at 268 nm[21] for C_2F_4BrI. The values obtained for C_2F_5I were 1.01 ± .05, 1.0 ± .04 and 1.04 ± .05 respectively and for C_2F_4BrI the value was .96 ± .04. Such large values for the I^* quantum yield indicate that, in all of

these molecules, the parallel $^3Q_0$ <- N transition is very much stronger than the perpendicular $^3Q_1$ <- N and $^1Q_1$ <- N transitions.

Our experimental results on C_2F_5I and C_2F_4BrI are summarized in Table 3. These results are consistent with the assumption that I^* is produced exclusively at 248 nm and 266 nm via the parallel $^3Q_0$ <- N transition. First, the derived c.m. angular distributions for C_2F_5I and C_2F_4BrI are both very close to the simple $\cos^2\theta$ distribution expected for a pure parallel transition (for C_2F_5I $\beta = 1.87$ at 248 nm; for C_2F_4BrI $\beta \approx 1.8$ at 266 nm and $\beta \approx 1.84$ at 248 nm.) Second, the product translational energy distributions in Figs. 4, 9 and 13 show no evidence of the bimodality which might be expected if both ground and excited state iodine atoms were being produced. In the case of C_2F_5I at 266 nm, a comparison between the C_2F_4Br velocity distribution and the I distribution demonstrated that all or almost all I^* is formed. In the case of C_2F_4BrI, our observation that some of the C_2F_4Br primary products do <u>not</u> spontaneously decompose provides additional evidence that excited rather than ground state iodine atoms are formed (see Sec. IIIC).

For both C_2F_5I and C_2F_4BrI, when the C-I bond breaks, approximately half of the 41 kcal/mole (or 33 kcal/mole at 266 nm) of available energy appears as product translational energy. The extent of translational energy release can be gauged by comparing to the predictions of two limiting impulsive models for photodissociation reactions.[17] In the "rigid radical limit," the iodine atom is pictured as recoiling from a completely rigid polyatomic radical. In this limit no vibrations of the radical are excited, and the maximum possible recoil energy is achieved. (The available energy is partitioned solely between product recoil

energy and rotational energy of the polyatomic radical, subject to the constraint of conservation of angular momentum). In the "soft radical limit," the iodine atom is pictured as recoiling only against the carbon atom (with the full available energy). The carbon atom then runs into the rest of the polyatomic radical, exciting the vibrational and rotational degrees of freedom of the radical fragment. The soft radical limit gives the minimum possible recoil energy for a given available energy (in the context of an impulsive model). For C_2F_5I, we calculated $f_T = 0.82$ in the rigid radical limit, and $f_T = 0.18$ in the soft radical limit, with similar values for C_2F_4BrI. The experimental values of $f_T = 0.51$ for C_2F_5I at 248 nm and $f_T = 0.48$ for C_2F_4BrI at 248 nm and 0.53 at 266 nm lie about halfway in between the rigid and soft radical limits. The fact that f_T is only slightly lower for C_2F_4BrI than for C_2F_5I indicates that the C_2F_4Br radical really isn't much "softer" than the C_2F_5 radical. Note, however, that the width of the product translational energy distribution is much greater in the case of C_2F_4BrI than in the case of C_2F_5I. Normally one might expect a wider translational energy distribution since C_2F_4Br has more low frequency modes than C_2F_5, but the presence of low frequency modes should also decrease the average recoil energy significantly, which was not observed. A simple explanation for a wider translational energy distribution for C_2F_4BrI than for C_2F_5I might also be that C_2F_4BrI dissociates with a much larger range of exit impact parameters (b) but the same average b. However, if this were the case one would also expect the c.m. angular distribution of the products to be more smeared out for C_2F_4BrI than for C_2F_5I, which it is not. Thus, we cannot explain the differences between the C_2F_5I and C_2F_4BrI P(E)'s with these usual simple kinematic models.

It has been known for some time that the I^* quantum yields in the (non-fluorinated) alkyl iodides tend to be lower than in the corresponding perfluorinated compounds. (Compare, for example, the broad-band data in Table I of Ref. 24). A priori, it is not obvious whether these differences result from different transition strengths to the $^3Q_1$, $^3Q_0$ and $^1Q_1$ components of the Q-complex, or from some other cause. However, in the case of CH_3I, the MCD results of Gedanken and Rowe[17] and the molecular beam photofragmentation results of Riley and Wilson[18,19] clearly show that, at 266 nm, absorption occurs almost exclusively to the $^3Q_0$ state; therefore, the production of ground state I atoms has to be ascribed to some sort of curve-crossing effect. Why curve crossing should be less important in the perfluorinated compounds is not clear.[38]

Even the heavily studied CH_3I molecule cannot be said to be fully understood. A molecular beam study of CH_3I at 248 nm might prove very interesting. The MCD results indicate that the $^1Q_1$ <- N transition should be important at 248 nm, accounting for at least 1/3 of the absorption. However, PBL measured an I^* quantum yield of 0.81 ± 0.03 at 248 nm, which is about the same as the value Riley and Wilson measured at 266 nm. If both of these results are correct, then at 248 nm one should see: I^* atoms formed with a parallel polarization dependence (absorption to $^3Q_0$, no curve crossing); I atoms formed with a parallel polarization dependence (absorption to $^3Q_0$ followed by curve crossing); I^* atoms formed with a perpendicular polarization dependence (absorption to $^1Q_1$ followed by curve crossing); and I atoms formed with a perpendicular polarization dependence (absorption to $^1Q_1$, no curve crossing). In cases such as this, it is clearly very important to distinguish between

the electronic states of the molecule which are initially excited, and the product electronic states which are finally formed.

B. C_2F_5Br at 193 nm

The situation for the alkyl bromides is qualitatively the same as for the alkyl iodides. In the absence of curve crossing effects, Br^* atoms should be formed via a parallel $^3Q_0$ <- N transition, and ground state Br atoms should be formed via perpendicular $^3Q_1$ <- N and $^1Q_1$ <- N transitions. The major quantitative difference is that the spin-orbit coupling is weaker in bromine than in iodine. This should cause the strengths of the $^3Q_0$ <- N and $^3Q_1$ <- N transitions to decrease, without much affecting the strength of the $^1Q_1$ <- N transition. Relatively low Br^* quantum yields would be expected in this case, although curve crossing processes could again foul things up.

In the case of CH_3Br, both the MCD spectrum[17] and the Br^* quantum yield[25] have been measured. Gedanken and Rowe[17] could not even detect the transitions to the $^3Q_1$ and $^3Q_0$ states in the MCD spectrum; only $^1Q_1$ <- N was observed. Ebenstein et al.[25] used atomic absorption spectroscopy to measure the relative yields of Br and Br^* following broad-band flash photolysis of a number of alkyl and perfluoroalkyl bromide molecules, and they obtained a broad-band Br^* quantum yield of 0.15 ± 0.12 for CH_3Br. The almost exclusive production of ground state bromine atoms is consistent with the $^1Q_1$ <- N assignment of Gedanken and Rowe, and suggests that curve crossing is not too important in the case of CH_3Br. Very low (< 10%) Br^* quantum yields were also obtained for C_2H_5Br and n-C_3F_7Br.

However, Ebenstein et al. observed much higher broad-band Br^* quantum yields for CF_3Br and C_2F_5Br (0.66±0.07 and 0.48±0.02, respectively). Without additional information, it is impossible to decide whether the increased Br^* production in CF_3Br and C_2F_5Br is due to an increase in strength of the $^3Q_0$ <- N transition, or curve-crossing effects, or both. Wavelength-specific values of the Br^* quantum yields for CF_3Br, C_2F_5Br, and also 1,2-C_2F_4BrI at 193 nm have been reported by PBL.[20] The values 0.56±0.05, 0.16±0.08, and 0.07±0.05, respectively, were obtained. In PBL's experiments, relative yields were obtained by monitoring the infrared emission from Br^*, and absolute yields were obtained by an indirect referencing procedure. (They assumed an I^* quantum yield of unity for n-C_3F_7I, and then they referenced their measured Br^* emission signals at 193 nm to the I^* emission signal from n-C_3F_7I at 308 nm). PBL point out that large systematic errors could be caused by this indirect referencing method, since it was necessary to change both the photolysis wavelength and the interference filter on the infrared detector to measure the n-C_3F_7I reference point. The Br^* quantum yield value of 0.56±0.05 obtained by PBL for CF_3Br at 193 nm happens to agree quite well with the broad-band value 0.66±0.07 obtained by Ebenstein et al. PBL argue that there should be good agreement between single-wavelength and broad-band photolysis determinations in the case of CF_3Br, since the CF_3Br absorption peak near 200 nm appears "fully resolved." This argument is not convincing. The CH_3I absorption band near 260 nm also appears "fully resolved," whereas in reality it contains three overlapping components. Since PLB's I^* quantum yield measurement in the photodissociation of C_2F_4BrI at 193 nm was found to be erroneous,[21] PBL's Br^* quantum yields measurements on C_2F_5Br, as well as on the other systems

included in their paper, need to be re-examined. The Br^* quantum yields of C_2F_4BrI at 193 nm was updated to be 0.14 ± 0.04[20] recently.

Unfortunately, our experimental results on C_2F_5Br provide little insight into what is going on. All we can say is that C-Br bond fission occurs at 193 nm, and that the mean C_2F_5 + Br recoil energy is around 30 kcal/mole. The measured Br^+ TOF distribution shows no evidence of bimodality, but the data quality is poor. Also, since the fine-structure splitting in bromine is only 10.5 kcal/mole, there might not be a large enough difference in the average translational energy release to resolve the Br and Br^* channels in the Br^+ TOF distribution if both are actually present. In Table 3, values of E_{avl} and f_T are listed for both possible product channels, reflecting our uncertainty on this point. It is unfortunate that we did not measure the relative Br^+ signal level at a few laboratory angles, in order to get at least a rough idea of the value of the asymmetry parameter for reaction (1). The asymmetry parameter, of course, would reveal whether the $^1Q_1$ or $^3Q_0$ state is mainly responsible for the absorption at 193 nm. It would be desirable, in the future, to return to C_2F_5Br and do the experiment properly. Comparative studies of CF_3Br, CH_3Br and C_2H_5Br would also be of interest.

C. 1,2-C_2F_4BrI at 193 nm

Consider first the C-Br fission reaction. The translational energy release observed for this reaction ($\overline{E}_T$ = 25.5 kcal/mole, FWHM = 9.0 kcal/mole) is similar to that observed for C_2F_5Br ($\overline{E}_T$ = 30 kcal/mole, FWHM = 11 kcal/mole). The smaller average value in 1,2-C_2F_4BrI might be due to larger exit impact parameter for the dissociation. The β value of 1.85 tells us that the electronic transition which leads to C-Br bond

fission is polarized parallel to the C-Br bond, which suggests that we are initially exciting the $^3Q_0$ component of the Q-complex on the C-Br bond. Why $^3Q_0$ <- N should be so strong in C_2F_4BrI, while it is undetectable in CH_3Br, is a mystery. Of course, $^3Q_0$ correlates to Br^* product. As mentioned in part B, Wight and Leone[21] measured a revised Br^* quantum yield of 0.14 ± 0.04 for C_2F_4BrI at 193 nm. We now know that C-Br bond fission accounts for only 1/3 of the total dissociation yield. Therefore, the fractional yield of Br^* (i.e., $[Br^*]/[Br^*]+[Br]$) will be 3 times greater than the Br^* quantum yield. This correction makes it plausible that quite a large fraction (but probably not more than half) of the C-Br dissociation events actually lead to Br^* product. Evidently, whatever ground state Br atoms are formed must be chalked up to curve-crossing processes.

We now turn to the unanticipated C-I bond fission reaction of C_2F_4BrI at 193 nm. Our results indicate that C-I bond fission outweighs C-Br bond fission by a 1.7:1 ratio. The asymmetry parameter for the C-I fission reaction is again close to two, which tells us that the electronic transition which leads to C_2F_4Br + I products is polarized parallel to the C-I bond. PBL observed no I^* emission whatsoever when they irradiated C_2F_4BrI at 193 nm. But the revised value of 0.50 ± 0.14 for the I^* quantum yield is very close to our dissociation yield of 0.64. If the secondary reaction (7) only produces ground state I, then this correspondence means that almost all the iodine atoms produced as I^* in the primary process (4a). The mean C_2F_4Br + I translational energy of 27 kcal/mole corresponds to only 37% of the available energy.

Unfortunately, we cannot offer a convincing explanation for the occurrence of C-I bond fission in C_2F_4BrI at 193 nm. It seems extremely unlikely that any component of the C-I Q-complex can be excited directly at 193 nm. The possibility of Rydberg transitions originating on the iodine atom must be considered. However, the Rydberg transitions in C_2F_5I do not start in until shorter wavelengths, and there is no obvious reason why the Rydberg transitions would be significantly shifted to longer wavelengths in C_2F_4BrI. Also, the transitions of non-bonding iodine electrons to Rydberg states would not, in general, be polarized parallel to the C-I bond.

An interesting possibility is that C-I bond fission might result from the <u>same</u> electronic transition which leads to C-Br bond fission. That is, after a component of the C-Br Q-complex is excited (presumably $^3Q_0$), a non-adiabatic transition to an electronic state correlating to C_2F_4Br + I products might occur. One can imagine that when the C-Br bond starts to separate along the electronically excited repulsive surface, some of the electronic energy will be converted into the kinetic energy of nuclear motion associated with the C-Br bond separation. At some C-Br separation, the electronic energy still remaining localized on the C-Br bond will become equal to the energy required to excite the n -> σ^* transition on the C-I bond. A near resonant intramolecular energy transfer could then occur, producing a new state of C_2F_4BrI which roughly consists of a locally electronically excited C-I bond and a vibrationally excited C-Br bond. This new state would dissociate immediately along the C-I repulsive surface. At the low temperatures of our molecular beam, most of the C_2F_4BrI molecules should be locked into

the gauche configuration. In the gauche configuration, the C-Br and C-I bonds are parallel. Then, an electronic transition polarized parallel to the C-Br bond could also lead to the formation of C_2F_4Br + I products with the experimentally observed angular distribution. If this explanation is correct, one would conclude that the initial excitation is, in fact, localized on the C-Br bond, and that the bond-selectivity is destroyed only by a curve crossing process.

At this stage, such "explanations" are little more than idle speculations. Much of the difficulty in interpreting the experiments performed so far is caused by: incomplete knowledge of the overlapping electronic transitions which contribute to the UV absorption spectrum; and the frequent occurrence of poorly understood curve crossings or intramolecular electronic energy transfer. As more MCD spectra, wavelength-specific quantum yield measurements, and molecular beam photofragmentation studies become available, a systematic understanding of the ultraviolet photodissociation of the alkyl halide molecules will emerge. Recent developments in tunable UV and VUV lasers should stimulate work in this area. It is not unreasonable to expect that, in the near future, the dream of bond-selective photochemistry will become a reality.

This work was supported by the Director, Office of Energy Research, Office of Basic Energy Sciences, Chemical Sciences Division of the U.S. Department of Energy under Contract No. DE-AC03-76SF00098. The excimer laser used in this research was a loan from the San Francisco Laser Center supported by the National Science Foundation under Grant No. CHE79-16250 awarded to the University of California at Berkeley in collaboration with Stanford University.

REFERENCES

1. R. S. Mulliken, J. Chem. Phys. 3, 375 (1935).

2. R. S. Mulliken, Phys. Rev. 46, 549 (1934).

3. R. S. Mulliken, Phys. Rev. 50, 1017 (1936).

4. R. S. Mulliken, Phys. Rev. 51, 310 (1936).

5. R. S. Mulliken, Phys. Rev. 47, 413 (1935).

6. M. Brith, M. D. Rowe, O. Schnepp, and P. J. Stephens, Chem. Phys. 9, 57 (1975).

7. The $A^3\Pi_{1_u}$, $B^3\Pi_{0_u}$ <- $X^1\Sigma_g^+$ transitions are forbidden in the absence of spin-orbit coupling, due to the selection rule $\Delta S = 0$ in Hund's cases (a) and (b). Spin-orbit coupling in the A and B states causes a partial transition to Hund's case (c), in which S is no longer a good quantum number. (In case (c), only Ω, the component of the total electronic angular momentum along the internuclear axis, is defined.)

8. R. J. Oldman, R. K. Sander, and K. R. Wilson, J. Chem. Phys. 54, 4127 (1971).

9. R. J. Oldman, R. K. Sander, and K. R. Wilson, J. Chem. Phys. 63, 4252 (1975).

10. T. G. Lindeman and J. R. Wiesenfeld, J. Chem. Phys. 70, 2882 (1979).

11. C. P. Hemenway, T. G. Lindeman, and J. R. Wiesenfeld, J. Chem. Phys. 70, 3560 (1979).

12. J. R. Wiesenfeld and R. H. Young, Chem. Phys. 58, 51 (1981).

13. H. Okabe, Photochemistry of Small Molecules (Wiley, 1978).

14. R. D. Clear, S. J. Riley, and K. R. Wilson, J. Chem. Phys. 63, 1340 (1975).

15. The ^3E state splits into four states, $A_1 + A_2 + E + E$. A_1 corresponds to $^3Q_0$ in Mulliken's notation, and one of the E states corresponds to $^3Q_1$. The ^1E state remains an E state, and corresponds to Mulliken's $^1Q_1$. See: G. Herzberg, Electronic Spectra and Electronic Structure of Polyatomic Molecules (Van Nostrand, 1966), pp. 17-18.

16. A. Gedanken and M. D. Rowe, Chem. Phys. Lett. 34, 39 (1975).

17. S. J. Riley and K. R. Wilson, Faraday Disc. Chem. Soc. 53, 132 (1972).

18. Since the R-X bond strength increases on going from X = I to Br to Cl, the energy separation between the R-X bonding σ M.O. and the R-X anti-bonding σ^* M.O. should also increase on going from I to Br to Cl. This effect will also contribute to the observed trend in the n -> σ^* transition energies.

19. S.J. Lee and R. Bersohn, J. Phys. Chem. 86, 728 (1982).

20. W. H. Pence, S. L. Baughcum, and S. R. Leone, J. Phys. Chem. 85, 3844 (1981).

21. C. A. Wight and S. R. Leone, J. Phys. Chem. 87, 5299 (1983).

22. R. N. Zare, Mol. Photochem. 4, 1 (1972).

23. G. E. Busch and K. R. Wilson, J. Chem. Phys. 56, 3638 (1972); S.-C. Yang and R. Bersohn, J. Chem. Phys. 61, 4400 (1974).

24. T. Donohue and J. R. Wiesenfeld, J. Chem. Phys. 63, 3130 (1975).

25. W. L. Ebenstein, J. R. Wiesenfeld, and G. L. Wolk, Chem. Phys. Lett. 53, 185 (1978).

26. V. S. Ivanov, A. S. Kozlov, A. M. Pravilov, and E. P. Smirnov, Sov. J. Quantum Electron. 10, 566 (1980).

27. J. B. Koffend and S. R. Leone, Chem. Phys. Lett. 81, 136 (1981).

28. C_2F_5Br was the last of the three molecules studied, and by that time the laser had become critically ill (as far as ArF was concerned).

29. K. C. Ferguson and E. Whittle, J. C. S. Faraday I, 68, 306 (1972).

30. The C-C bond strength in C_2F_5 was calculated using $\Delta H_f^o(C_2F_5) = -213$ kcal/mole (Ref. 30), $\Delta H_f^o(CF_3) = -112.4$ kcal/mole (Ref. 31), and $\Delta H_f^o(CF_2) = -43.5$ kcal/mole (Ref. 31).

31. E.-C. Wu and A. S. Rodgers, J. Am. Chem. Soc. 98, 6112 (1976).

32. JANAF Thermochemical Tables, 2nd ed., Natl. Stand. Ref. Data Ser., U.S. Natl. Bur. Stand. 37 (U.S. Government Printing Office, Washington, D.C., 1971).

33. The C_2F_4-Br and C_2F_4-I bond strengths were estimated as follows. The value $\Delta H_f^o(C_2F_5) = -213$ kcal/mole was taken from Ref. 30. The values $\Delta H_f^o(F) = 18.9$ kcal/mole, $\Delta H_f^o(Br) = 26.7$ kcal/mole, $\Delta H_f^o(I) = 25.5$ kcal/mole, and $\Delta H_f^o(C_2F_4) = -157.4$ kcal/mole were taken from Ref. 31 (JANAF). Using the values $D_o(C_2F_5\text{-}Br) = 68.6$ kcal/mole

(Ref. 28) and $D_o(C_2F_5\text{-}I)$ = 52.5 kcal/mole (Ref. 30), we calculated the heats of formation of C_2F_5Br and C_2F_5I: $\Delta H_f^o(C_2F_5Br)$ = -213 + 26.7 - 68.6 = -255 kcal/mole, $\Delta H_f^o(C_2F_5I)$ = -213 + 25.5 - 52.5 = -240 kcal/mole. We then assumed that the C-F bond dissociation energies in C_2F_5Br and C_2F_5I are the same as in C_2F_6. $D_o(C_2F_5\text{-}F)$ is known to be 127 kcal/mole (Ref. 30). This assumption allows us to estimate the heats of formation of the C_2F_4Br and C_2F_4I radicals: $\Delta H_f^o(C_2F_4Br)$ = -255 -18.9 + 127 = -147 kcal/mole, $\Delta H_f^o(C_2F_4I)$ = -240 -18.9 +127 = -132 kcal/mole. We obtain finally $D_o(C_2F_4\text{-}Br)$ = -157.4 + 26.7 + 147 = 16 kcal/mole, $D_o(C_2F_4\text{-}I)$ = -157.4 + 25.5 + 132 = 0 kcal/mole. In reality, the C-F bond dissociation energies in C_2F_5Br and C_2F_5I are probably somewhat lower than in C_2F_6. Therefore, the C_2F_4-Br and C_2F_4-I bond strengths may be somewhat higher than estimated above.

34. The activation energies for halogen atom addition to unsaturated hydrocarbons are typically very small. Therefore, the threshold energies for reactions (6) and (7) are not expected to be much higher than the endothermicities.

35. See, for example: D. Krajnovich, F. Huisken, Z. Zhang, Y. R. Shen, and Y. T. Lee, J. Chem. Phys. 77, 5977 (1982).

36. R. E. Center and A. Mandl, J. Chem. Phys. 57, 4104 (1972).

37. T. M. Miller and B. Bederson, Adv. At. Mol. Phys. 13, 1 (1977).

38. This curve crossing explanation for the lower I^* quantum yields in the (non-fluorinated) alkyl iodides does not rule out the additional possibility that the $^3Q_1$ <- N and $^1Q_1$ <- N transitions are

relatively less intense in the perfluorinated molecules.

39. E. Gerck, J. Chem. Phys. 79, 311 (1983).

Table 1. Parameters obtained by fitting measured beam number density velocity distributions to the form:

$$N(v) \propto v^2 \exp[-(\frac{v}{\alpha} - S)^2] \quad .$$

For this functional form, the peak (most probable) velocity is given by $v_{PK} = \frac{\alpha S}{2} [1 + \sqrt{1 + 4/S^2}]$. v and α are given in units of 10^4 cm/s.

Gas	Calibration #1			Calibration #2		
	α	S	v_{PK}	α	S	v_{PK}
C_2F_5Br	0.653	10.39	6.85	0.619	10.92	6.82
C_2F_5I	0.547	12.26	6.75	0.502	13.25	6.69
1,2-C_2F_4BrI (248 nm)	0.490	13.44	6.62	0.486	13.37	6.53
1,2-C_2F_4BrI (266 nm)	.459	14.07	6.49	0.461+	14.17+	6.53+

+This calibration was performed by depleting the molecular beam at the interaction region with the laser.

Table 2. Comparison of experimental and calculated laboratory angular distributions of primary I and Br products from C_2F_4BrI photodissociation at 193 nm. The experimental and calculated distributions have all been normalized to 1000 at $\Theta = 20°$.

Θ	I atom signal*				Br atom signal**			
	Experimental	Calculated			Experimental	Calculated		
		$\beta = 1.70$	$\beta = 1.85$	$\beta = 2.00$		$\beta = 1.70$	$\beta = 1.85$	$\beta = 2.00$
10°	1270 ± 57	1283	1307	1330	1217 ± 90	1218	1235	1252
20°	1000 ± 47	1000	1000	1000	1000 ± 77	1000	1000	1000
30°	558 ± 24	627	600	573	670 ± 50	679	675	655
40°	230 ± 19	283	243	203	385 ± 47	372	338	305

*Experimental numbers were obtained by integrating the signal in the measured I^+ TOF distributions between 120-180 μs. Error bars represent ±2 standard deviations. A triangular-shaped $P(E_T)$ [$\overline{E}_T$ = 27.0 kcal/mole, FWHM = 13.0 kcal/mole] for the reaction $C_2F_4BrI \rightarrow C_2F_4Br + I$ was used in the calculations.

**Experimental numbers were obtained by integrating the signal in the measured Br^+ TOF distributions between 90-140 μs. Error bars represent ±2 standard deviations. A triangular-shaped $P(E_T)$ [$\overline{E}_T$ = 25.5 kcal/mole, FWHM = 9.0 kcal/mole] for the reaction $C_2F_4BrI \rightarrow C_2F_4I + Br$ was used in the calculations.

Table 3. Summary of principal experimental results.

Reaction	Wavelength (nm)	$P(E_T)$ $\bar{E}_T$ (kcal/mole)	$P(E_T)$ FWHM (kcal/mole)	β	E_{avl} (kcal/mole)	$f_T = \frac{\bar{E}_T}{E_{avl}}$
(1) $C_2F_5Br \rightarrow C_2F_5 + (Br, Br^*)$	193	30	11	--	(79,69)	(0.38,0.43)
(2) $C_2F_5I \rightarrow C_2F_5 + I^*$	248	20.9	6.8	1.87	41	0.51
(3a) $C_2F_4BrI \rightarrow C_2F_4Br + I^*$	248	19.5	11.1	1.84	41	0.48
(3b) $C_2F_4BrI \rightarrow C_2F_4Br + I^*$	266	17.8	9.5	~1.8	33	.53
(4a) $C_2F_4BrI \rightarrow C_2F_4Br + (I, I^*)$	193	27.0	13.0	1.85	74	0.37
(4b) $C_2F_4BrI \rightarrow C_2F_4I + (Br, Br^*)$	193	25.5	9.0	1.85	(79,69)	(0.32,0.37)

FIGURE CAPTIONS

Fig. 1. C_2F_5Br, 193 nm. Laboratory TOF distribution of Br product at $\theta = 10°$. ○ Experimental points; ———— calculated using a trapezoidal-shaped $P(E_T)$ [E_T = 30 kcal/mole, FWHM = 11 kcal/mole] and the value $\beta = 2.0$.

Fig. 2. C_2F_5I, 248 nm. Laboratory TOF distributions of I atom product at four detector angles. ○ Experimental points; ———— calculated using the $P(E_T)$ in Fig. 4 and $\beta = 1.87$.

Fig. 3. C_2F_5I, 248 nm. Laboratory angular distribution of I atom product. ○ Experimental points, obtained by integrating and normalizing the TOF distributions in Fig. 2 (±2 error bars shown); the curves were calculated using the $P(E_T)$ in Fig. 4 and the following values of β: — — — $\beta = 1.77$; ———— $\beta = 1.87$; —— —— $\beta = 1.97$.

Fig. 4. Center-of-mass translational energy distribution for the products of C_2F_5I photodissociation at 248 nm. The distribution has a mean translational energy of 20.9 kcal/mole and a FWHM energy spread of 6.8 kcal/mole.

Fig. 5. C_2F_5I, 248 nm. Laboratory TOF distributions of $C_2F_5\cdot$ (C_2F_5 monitored as $C_2F_4^+$ in the mass spectrometer.) Symbols as in Fig. 2.

Fig. 6. C_2F_5I, 248 nm. Laboratory angular distribution of $C_2F_5\cdot$ (C_2F_5 monitored as $C_2F_4^+$ in the mass spectrometer.) Symbols as in Fig. 3.

Fig. 7. C_2F_4BrI, 248 nm. Laboratory TOF distributions of I atom product. ○ Experimental points; ———— calculated using the $P(E_T)$ in Fig. 9 and β = 1.84.

Fig. 8. C_2F_4BrI, 248 nm. Laboratory angular distribution of I atom product. ○ Experimental points, obtained by integrating and normalizing the TOF distributions in Fig. 7; ● experimental points from laboratory angular scans using dual channel scaler (±2 error bars shown on all experimental points); the curves were calculated using the $P(E_T)$ in Fig. 9 and the following values of β: — — — — β = 1.74; ———— β = 1.84; — — — — β = 1.94.

Fig. 9. Center-of-mass translational energy distribution for the products of C_2F_4BrI photodissociation at 248 nm. The distribution has a mean translational energy of 19.5 kcal/mole and a FWHM energy spread of 11.1 kcal/mole.

Fig. 10. C_2F_4BrI, 248 nm. Measured TOF distributions of the $C_2F_4^+$ and $^{79}Br^+$ mass spectrometer signals at $\Theta = 10°$. The arrow marks the position where C_2F_4Br would appear in the $C_2F_4^+$ TOF distribution if none of the C_2F_4Br radicals spontaneously decomposed.

Fig. 11. C_2F_4BrI, 266 nm. Laboratory TOF distributions of I atom product. ○ Experimental points; ———— calculated using the solid line $P(E_T)$ in Fig. 13 and β = 1.8.

Fig. 12. C_2F_4BrI, 266 nm. Laboratory angular distribution of I atom product. ○ Experimental points, obtained from integrating

some of the scans that were summed to give the data in Fig. 11, ▲ average of the experimental points. ($\pm 2\sigma$ error bars of the statistical counting error are shown on the average experimental points for the angles for which the error is larger than the size of the triangle.) Errors in keeping the beam intensity and lesser power constant were clearly larger). The curves were calculated using the solid line $P(E_T)$ in Fig. 12 and the following values of β: — — — $\beta = 1.6$, ——— $\beta = 1.8$, ——— ——— $\beta = 2.0$.

Fig. 13. Center-of-mass translational energy distribution for the products of C_2F_4BrI photodissociation at 266 nm. The total translational energy distribution is shown in solid line and was derived from the I^+ TOF data shown in Fig. 11. The translational energy distribution of the dissociation events that produced stable C_2F_4Br is shown in dotted line, scaled to lie under the solid line $P(E_T)$. This was obtained from fitting the sharp spike in the $C_2F_4^+$ TOF distribution shown in Fig. 14.

Fig. 14. C_2F_4BrI, 266 nm. Laboratory TOF distributions of $C_2F_4^+$ signal from C_2F_4Br primary product and C_2F_4 secondary product. ——— • ——— C_2F_4Br contribution calculated from the dotted line $P(E_T)$ in Fig. 13 and $\beta = 1.8$ — — — Assumed shape of underlying signal from C_2F_4 products from secondary dissociation of the slow C_2F_4Br product. ——— Sum of the C_2F_4Br and C_2F_4 contributions.

Fig. 15. C_2F_4BrI, 193 nm. TOP PANEL: ○ measured TOF distribution of the I^+ mass spectrometer signal at $\Theta = 10^\circ$; ———— I atom TOF distribution calcualted assuming a symmetric, triangular-shaped $P(E_T)$ [$\bar{E}_T$ = 27.0 kcal/mole, FWHM = 13.0 kcal/mole] and the value β = 1.85 for the reaction $C_2F_4BrI \rightarrow C_2F_4Br + I$. BOTTOM PANEL: ○ measured TOF distribution of the Br^+ mass spectrometer signal at $\Theta = 10^\circ$; ———— Br atom TOF distribution calculated assuming a symmetric, triangular-shaped $P(E_T)$ [$\bar{E}_T$ = 25.5 kcal/mole, FWHM = 9.0 kcal/mole] and the value β = 1.85 for the reaction $C_2F_4BrI \rightarrow C_2F_4I + Br$.

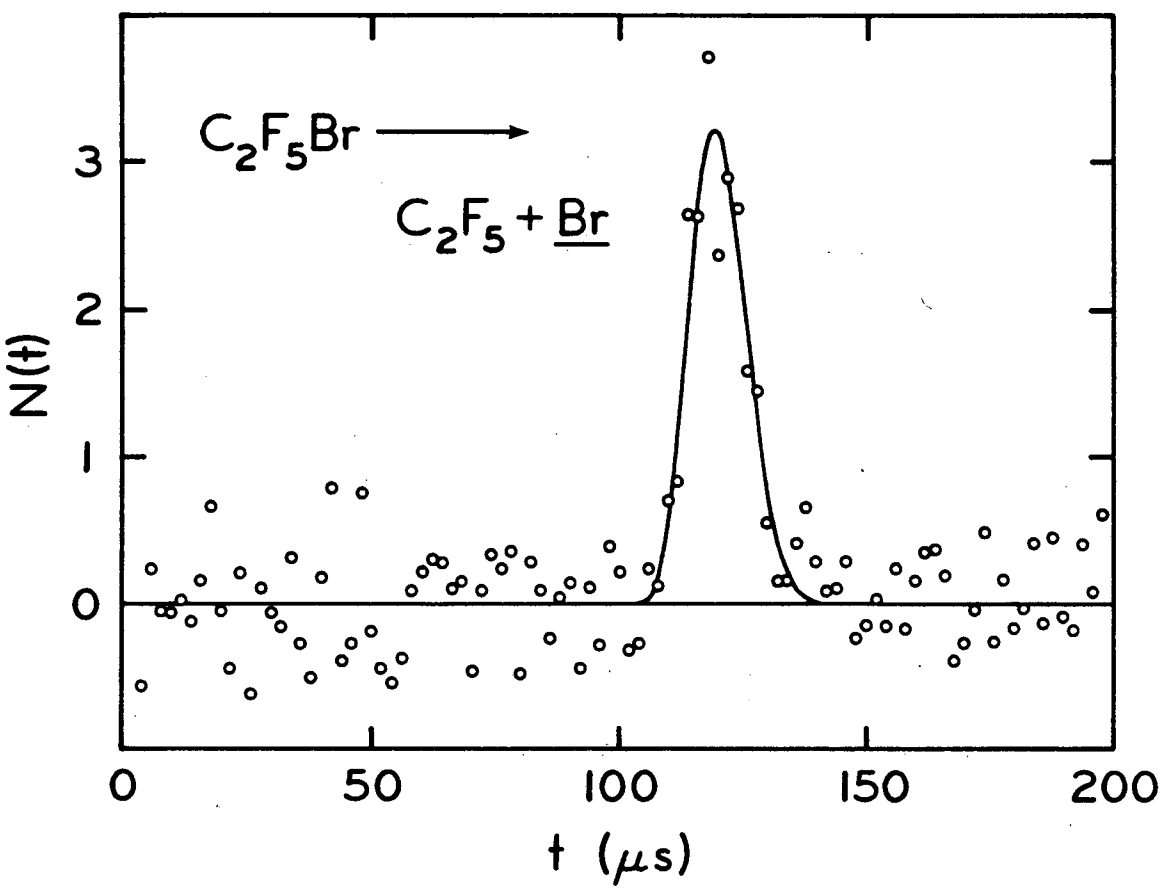

XBL 831-7684

Fig. 1

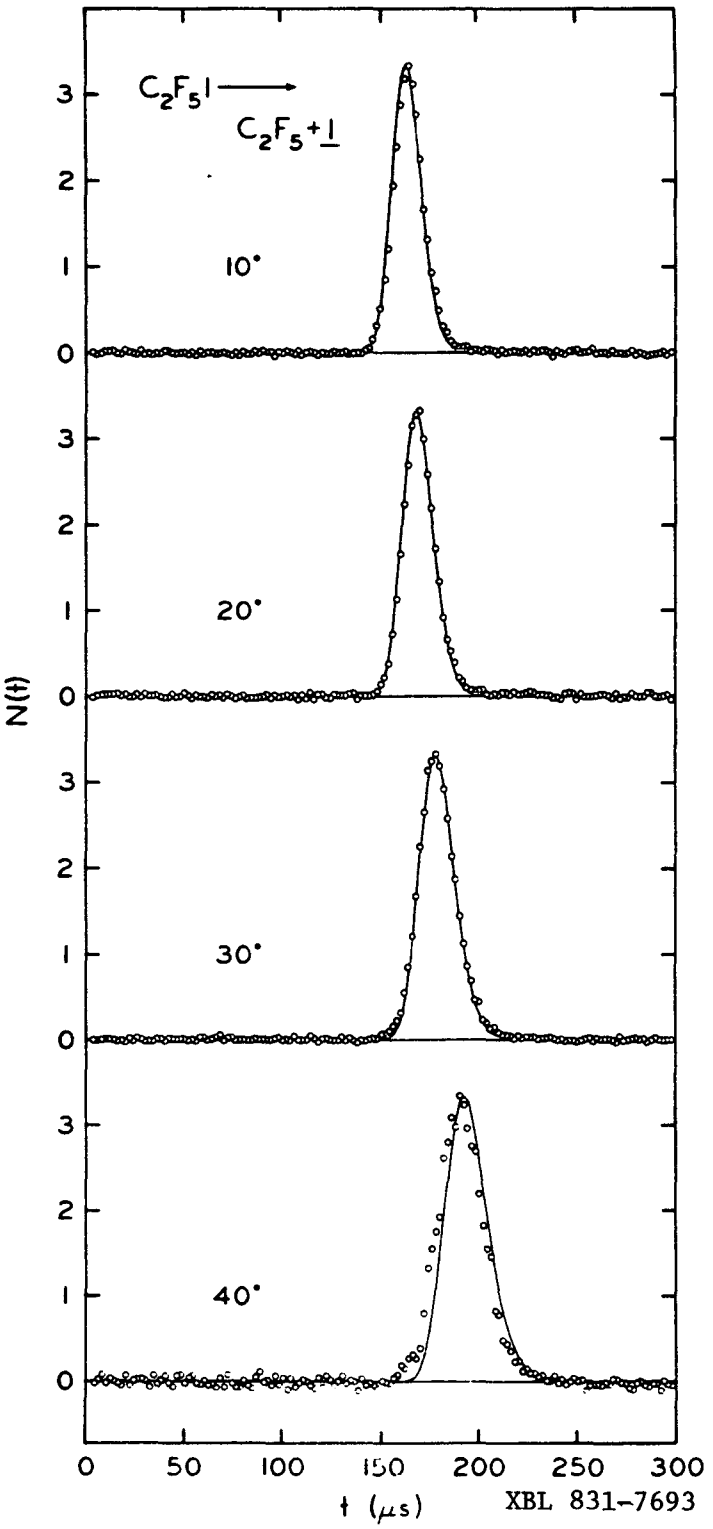
$C_2F_5I \longrightarrow C_2F_5 + I$
10°
20°
30°
40°
N(t)
0
1
2
3
0
50
100
150
200
250
300
t (μs)
XBL 831-7693

Fig. 2

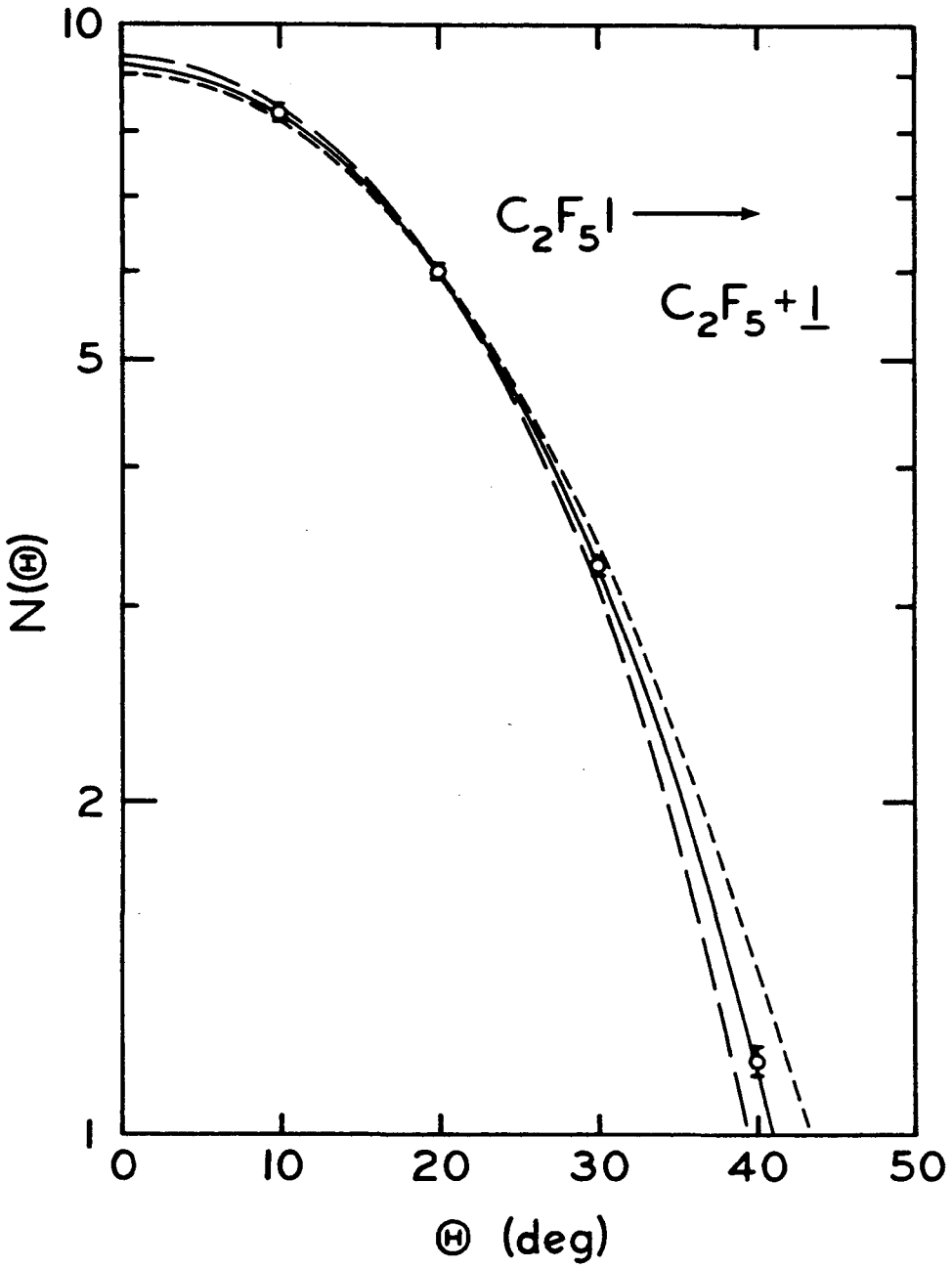

XBL 831-7687

Fig. 3

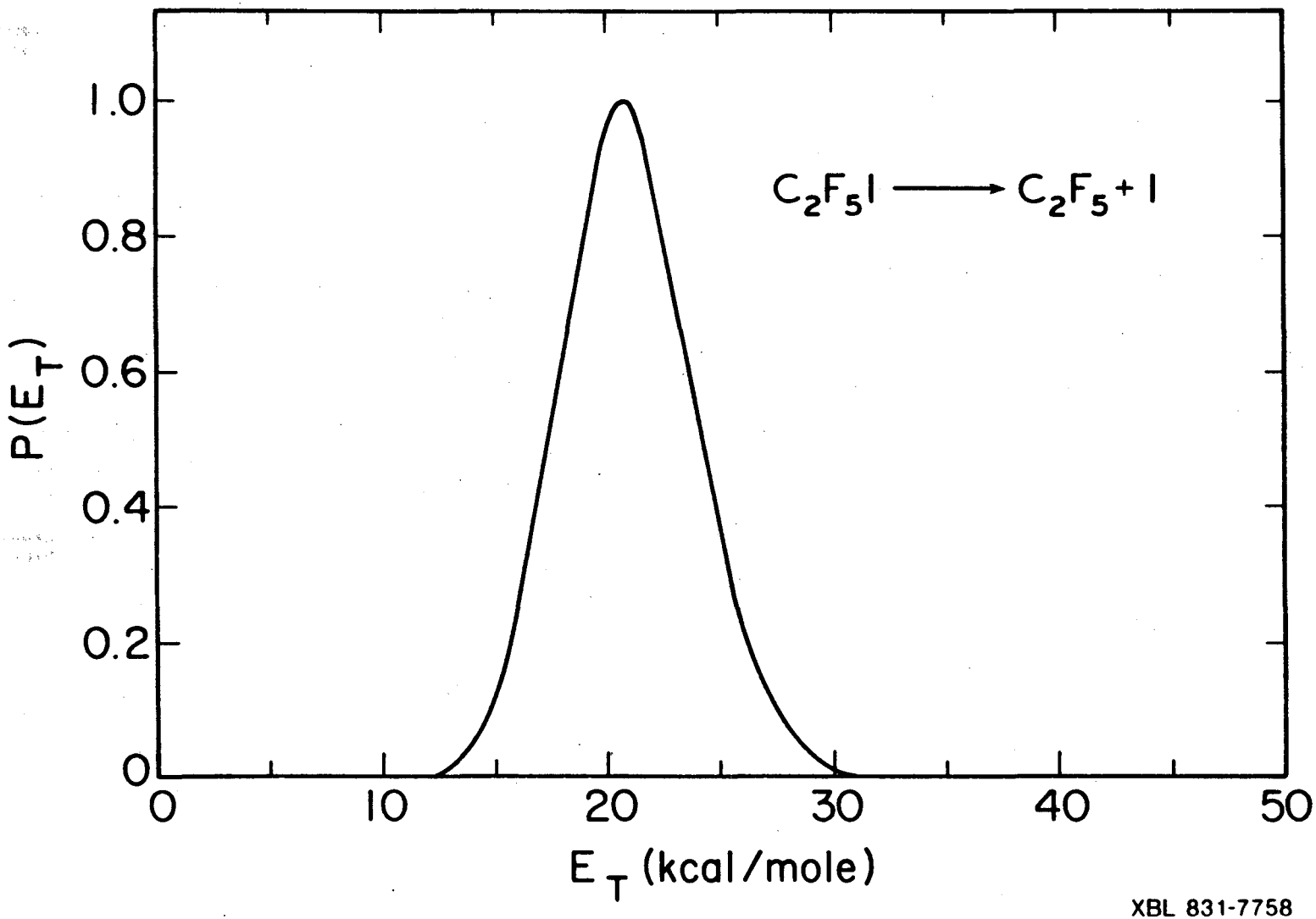

XBL 831-7758

Fig. 4

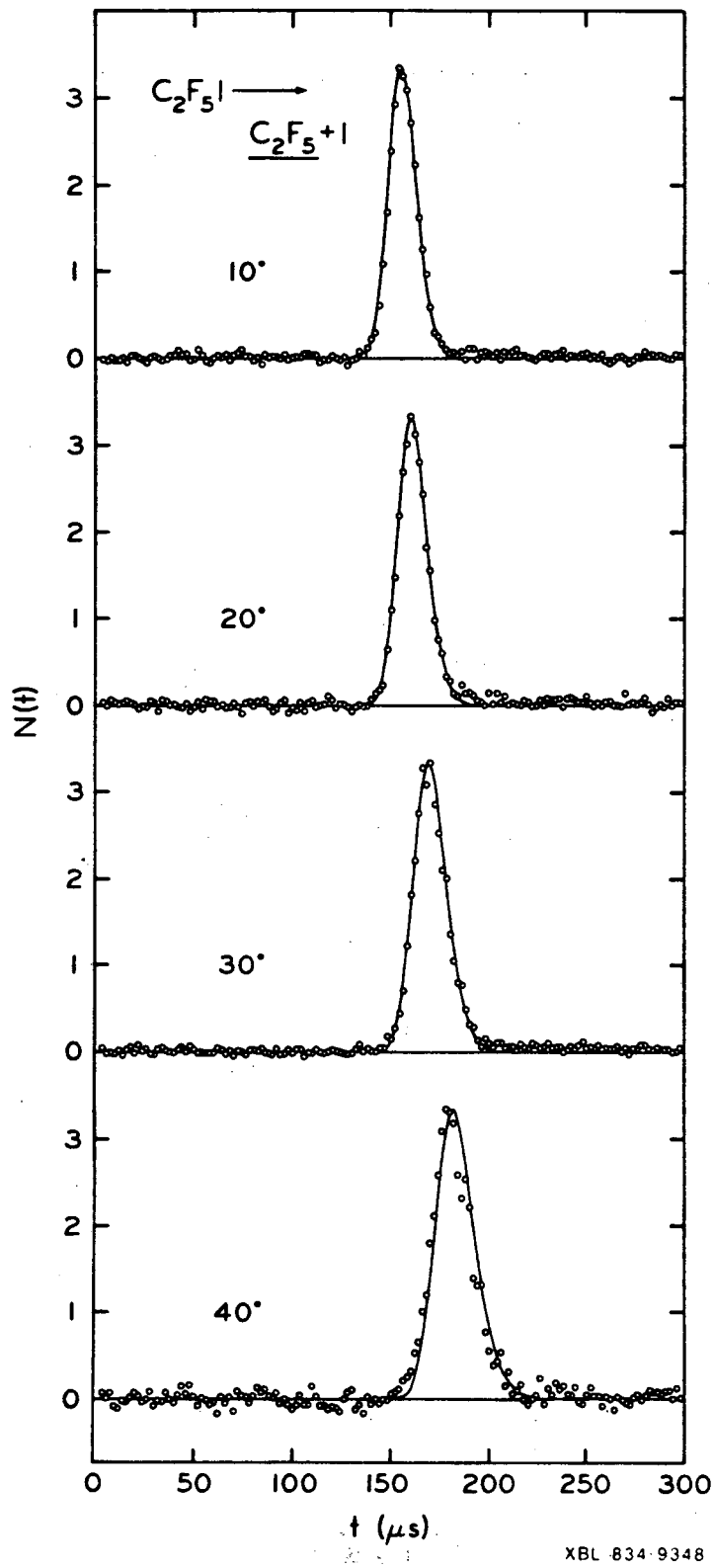
$C_2F_5I \longrightarrow$
$\underline{C_2F_5}+I$
10°
20°
30°
40°
N(t)
0
1
2
3
0
50
100
150
200
250
300
t (μs)
XBL 834-9348

Fig. 5

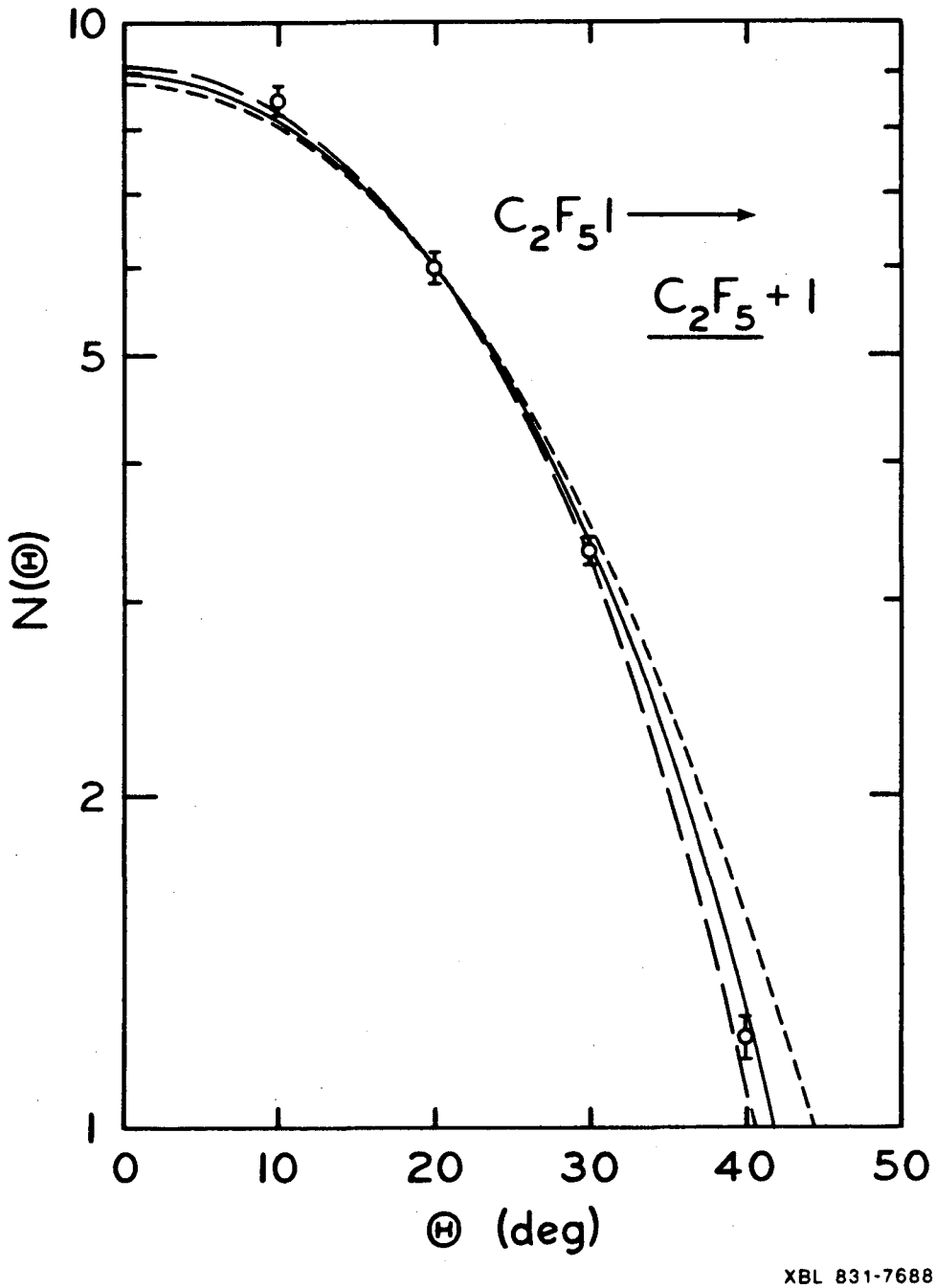
10
5
2
1
0
10
20
30
40
50
N(Θ)
Θ (deg)
$C_2F_5I \longrightarrow$
$\underline{C_2F_5} + I$
XBL 831-7688

Fig. 6

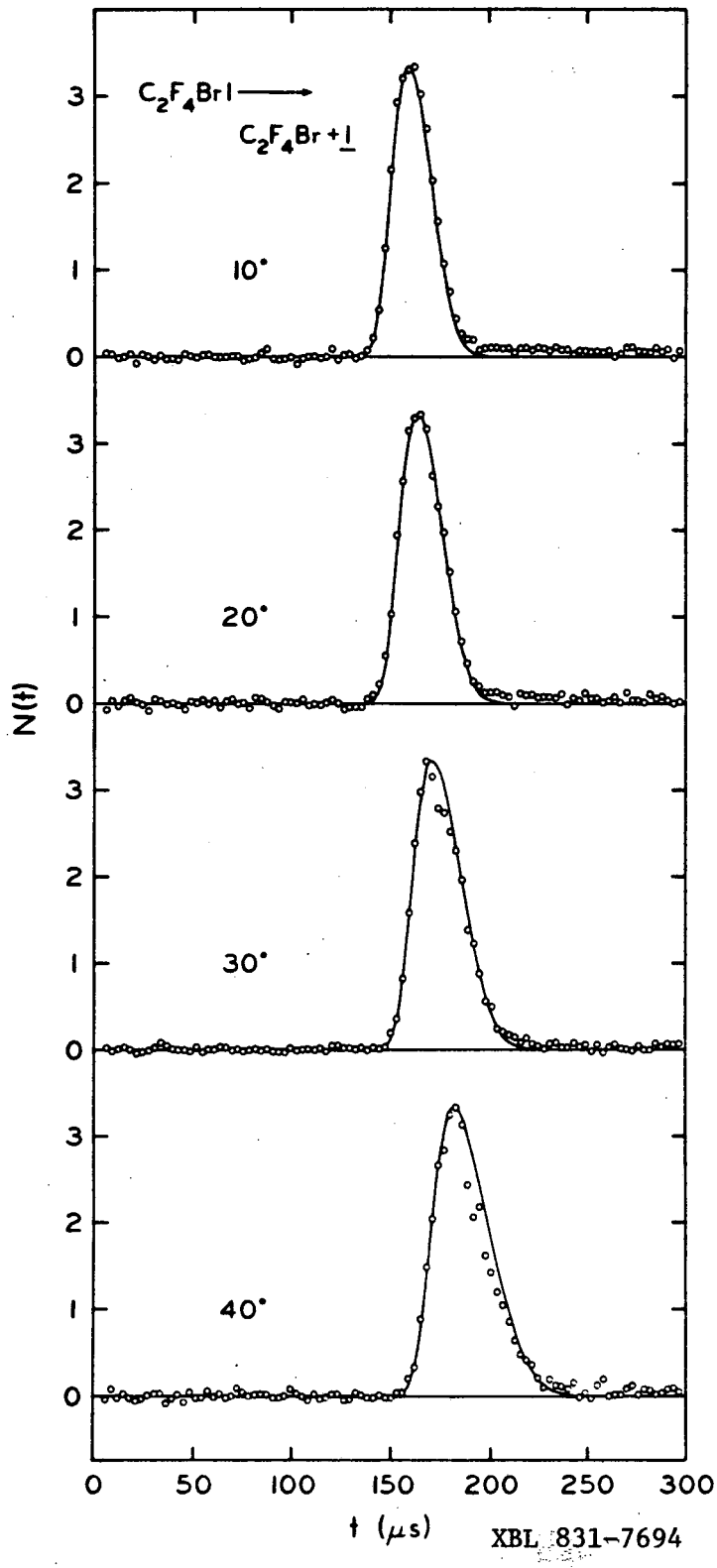
$C_2F_4BrI \longrightarrow$
$C_2F_4Br + \underline{I}$
10°
20°
30°
40°
N(t)
0
1
2
3
0
50
100
150
200
250
300
t (μs)
XBL 831-7694

Fig. 7

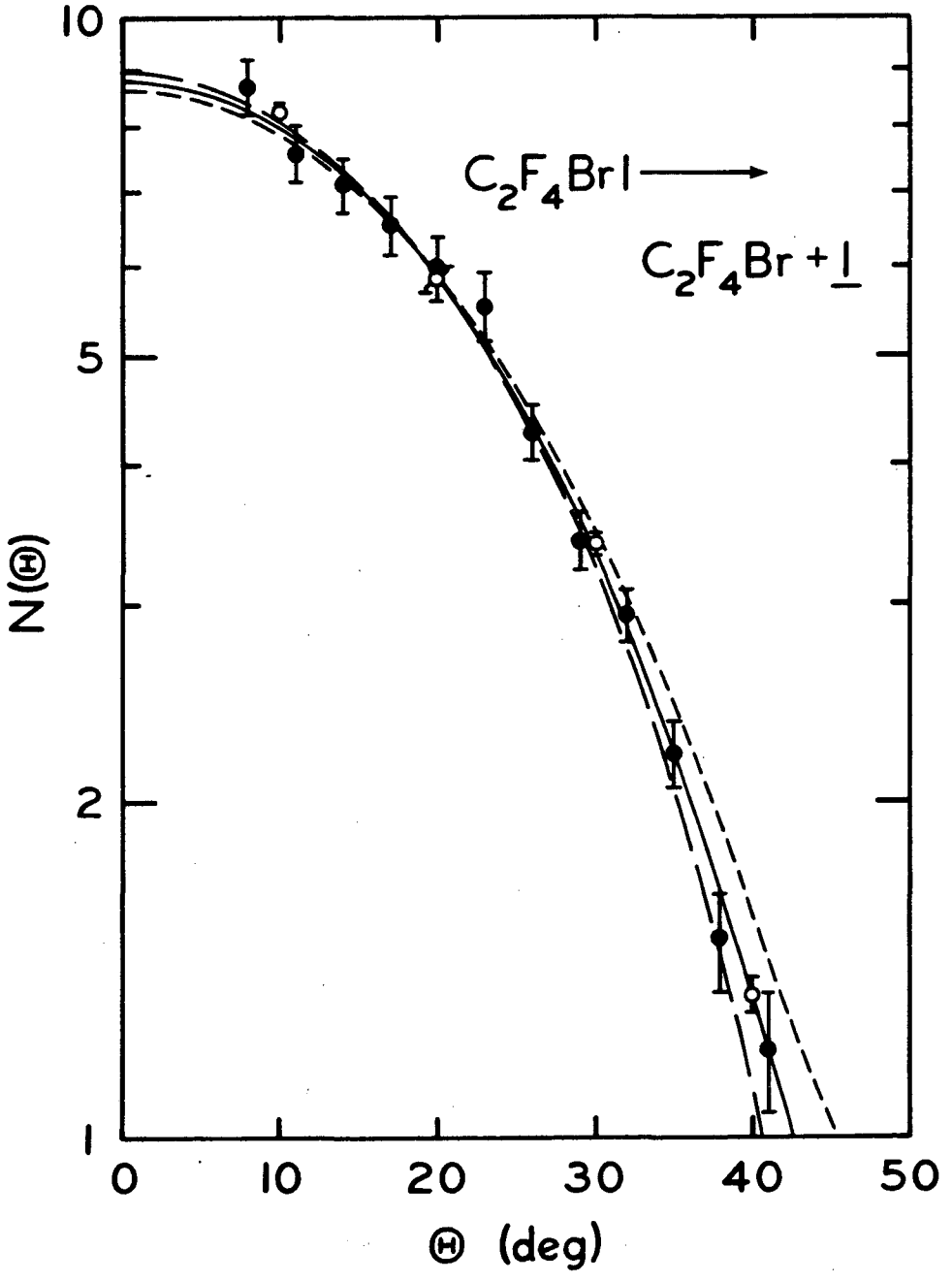

XBL 831-7689

Fig. 8

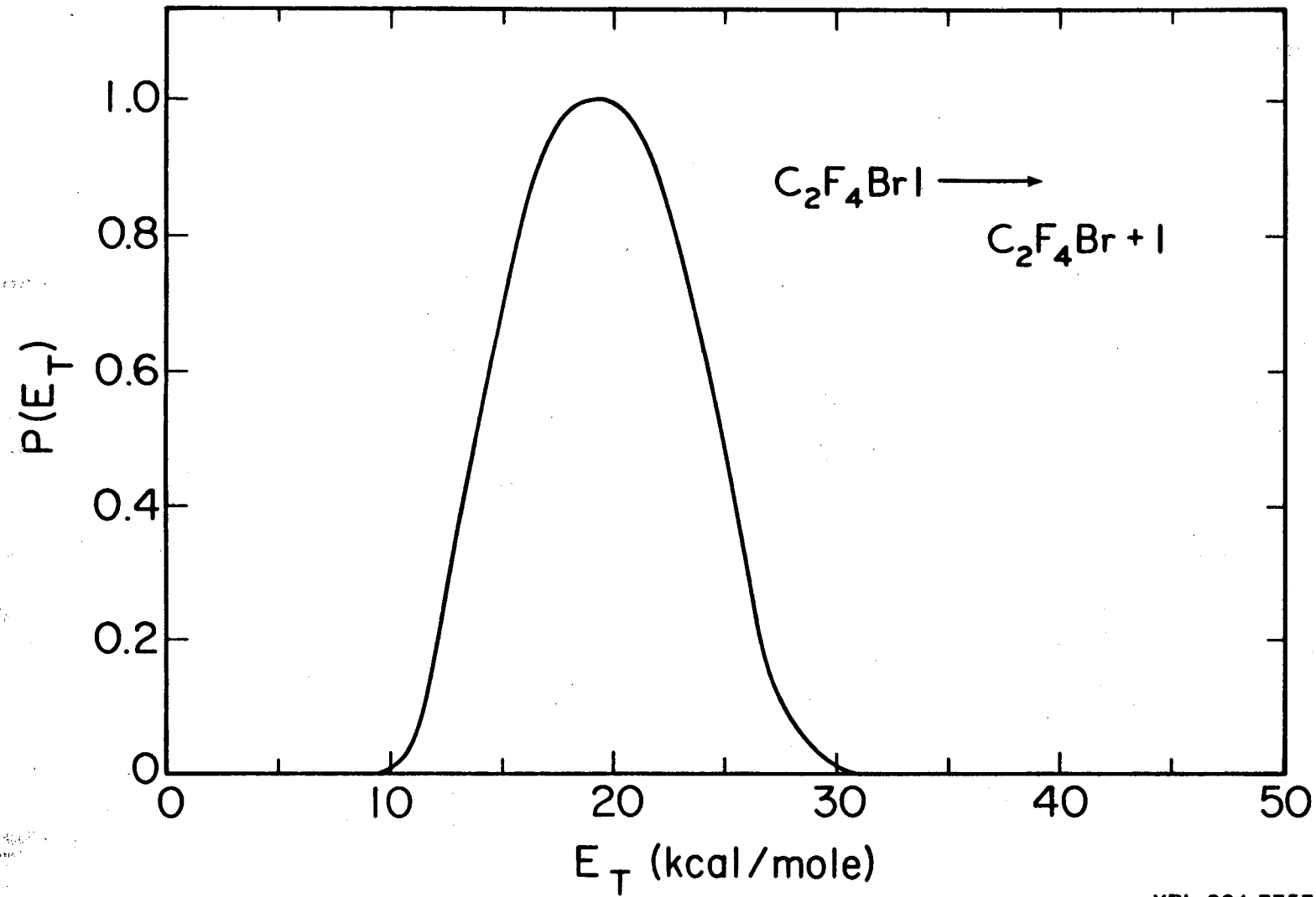

XBL 831-7757

Fig. 9

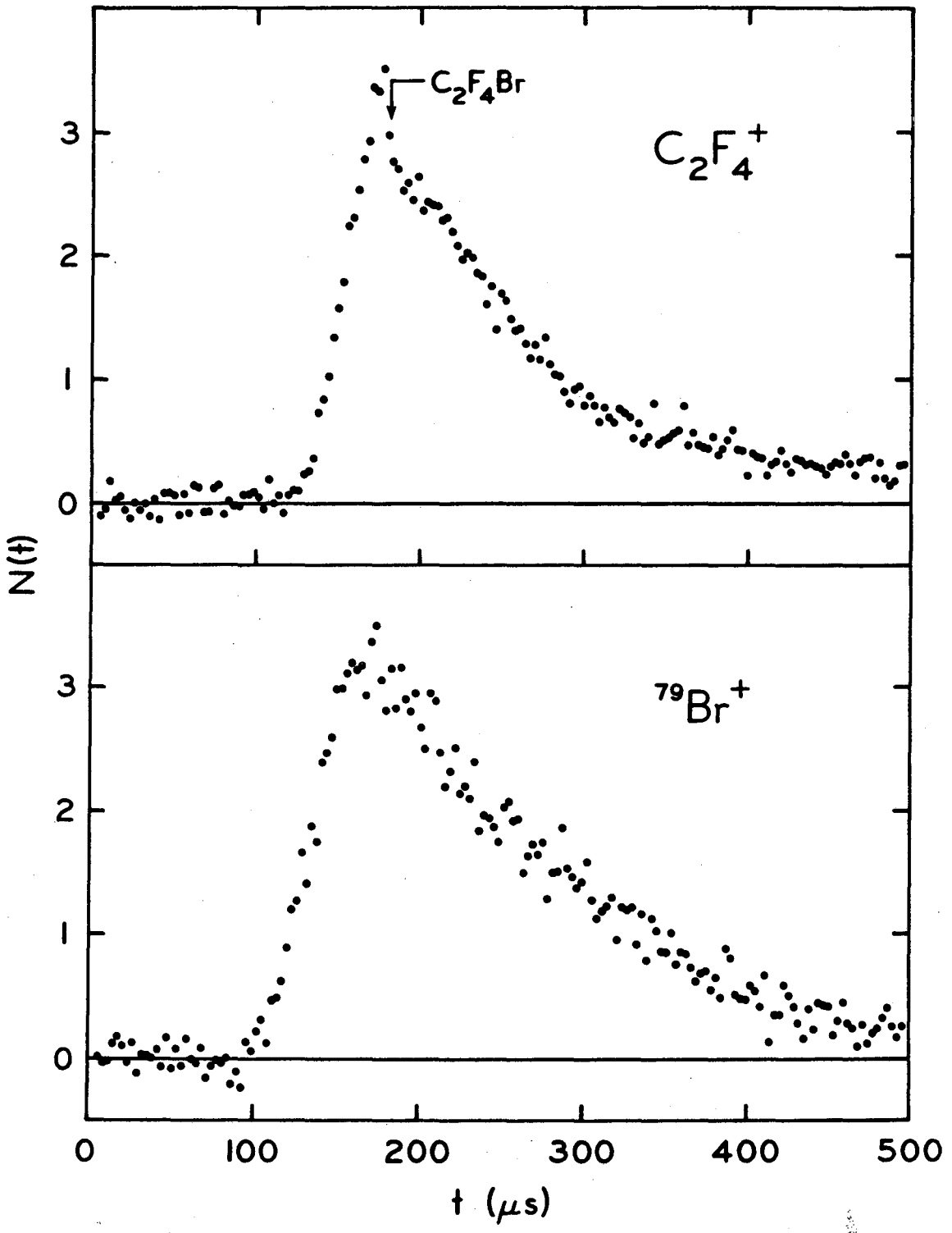

XBL 831-7695

Fig. 10

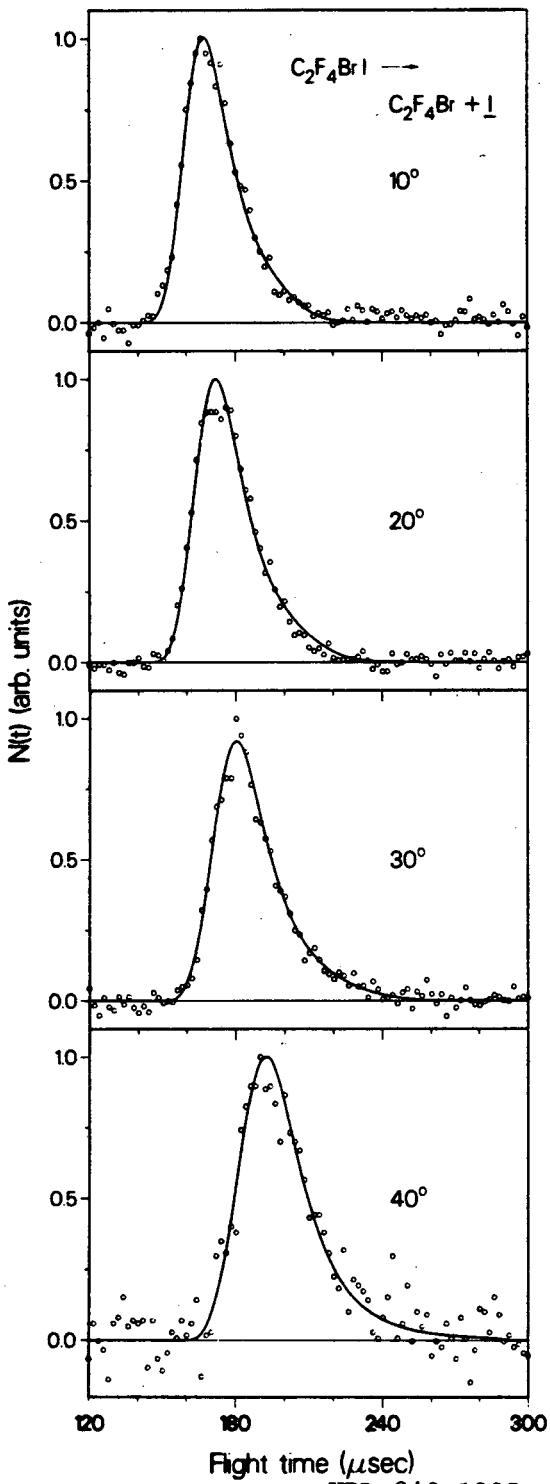

XBL 843-1225

Fig. 11

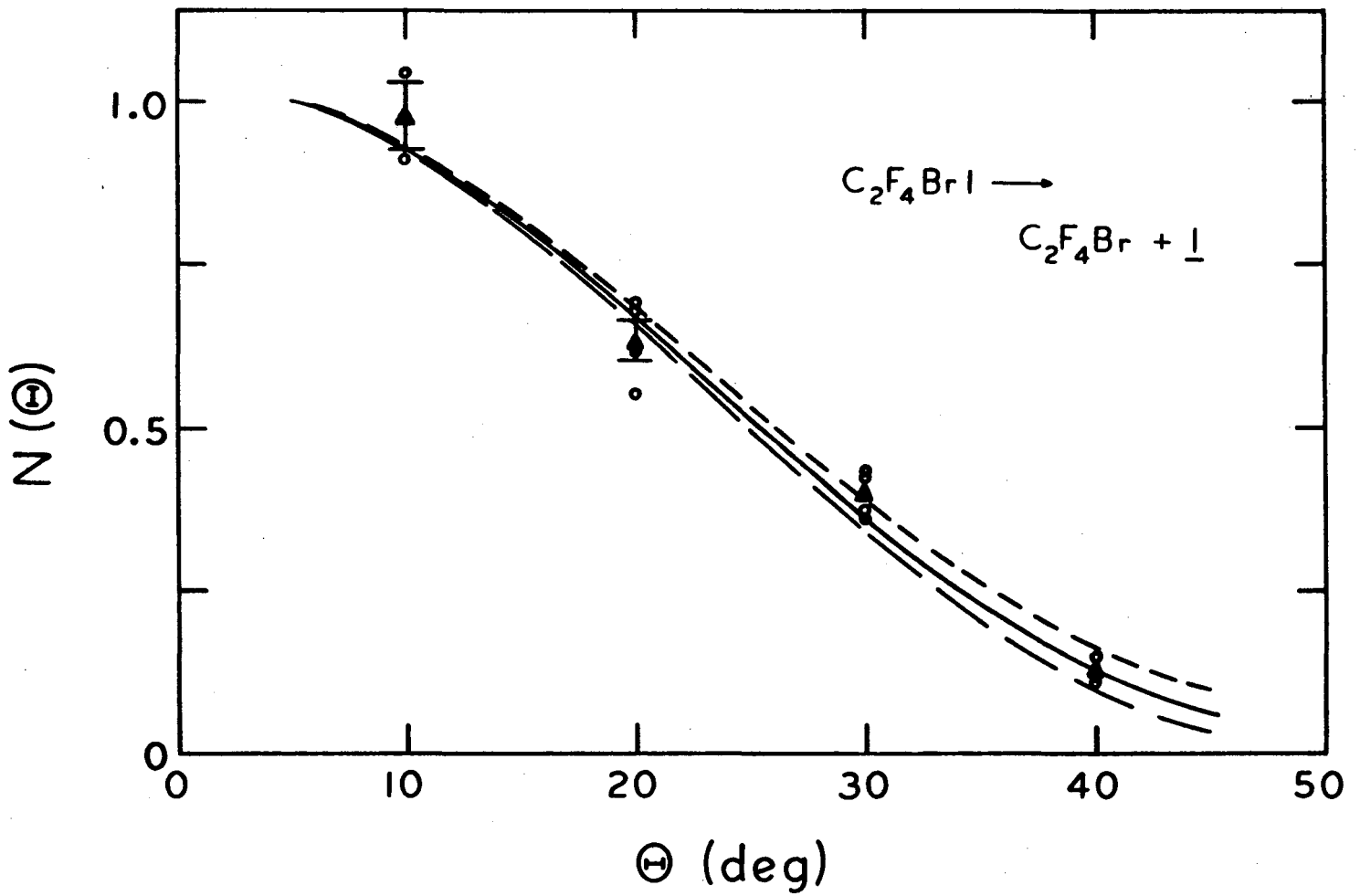

XBL 843-1222

Fig. 12

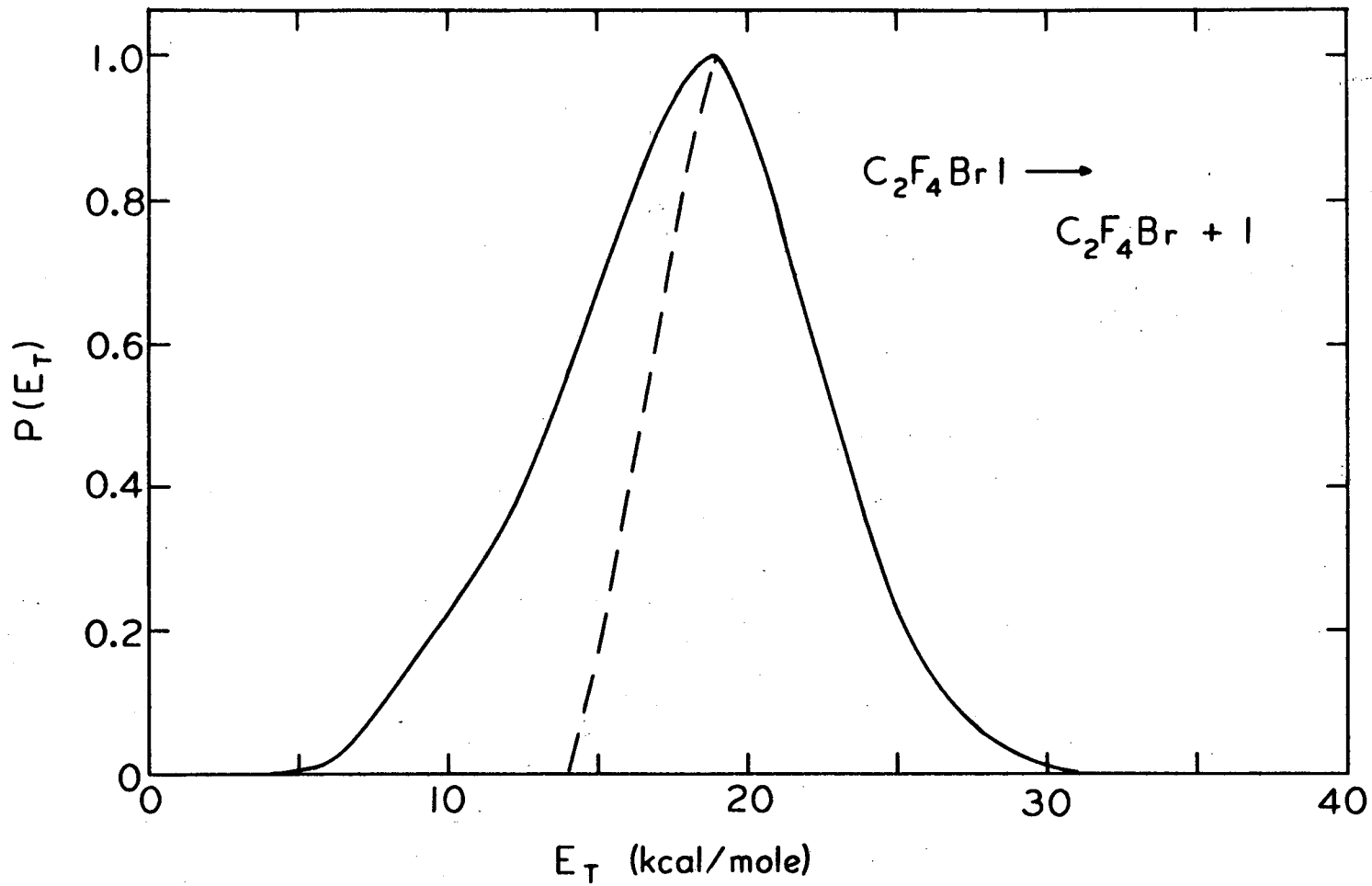

XBL 843-1224

Fig. 13

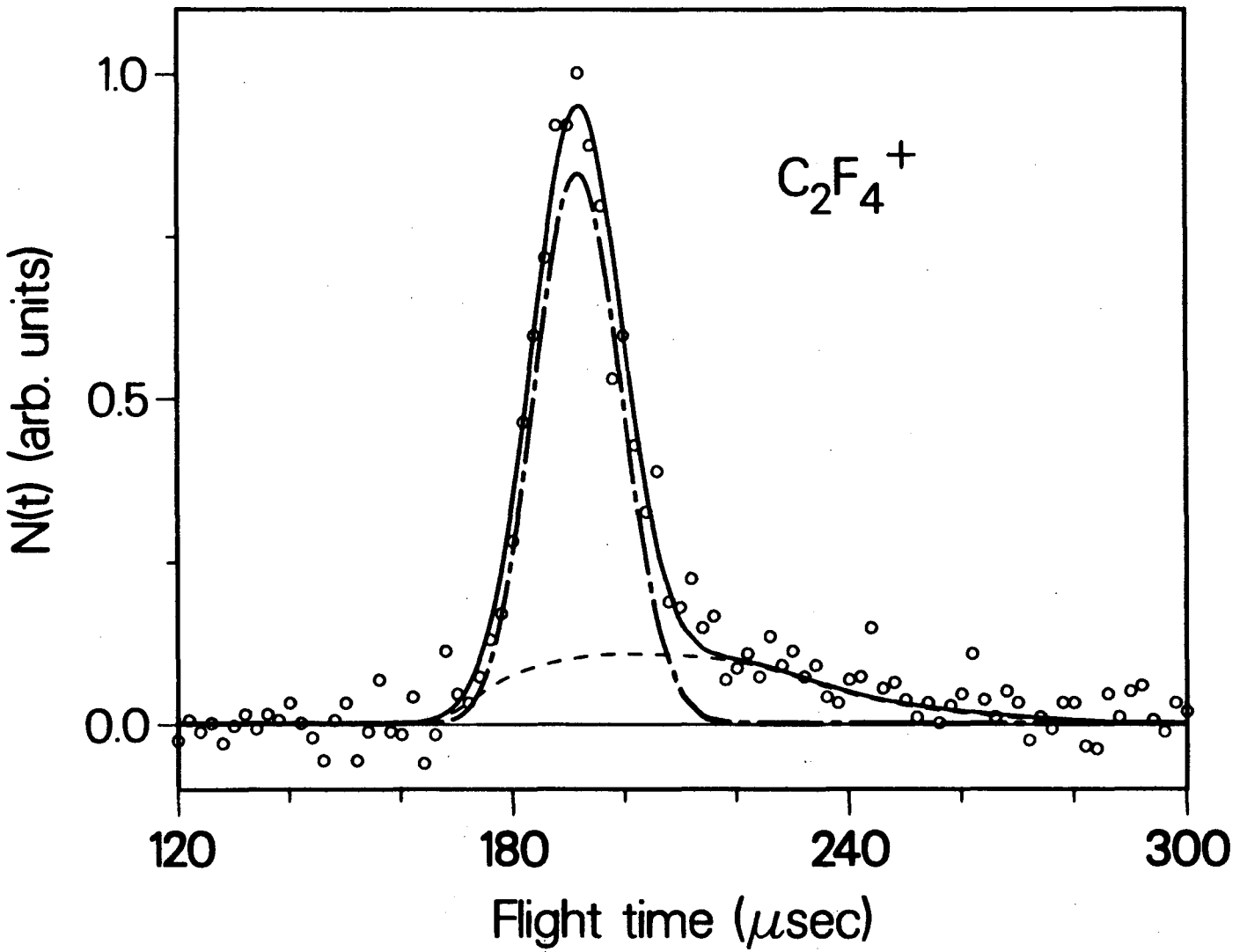

Fig. 14

XBL 843-1223

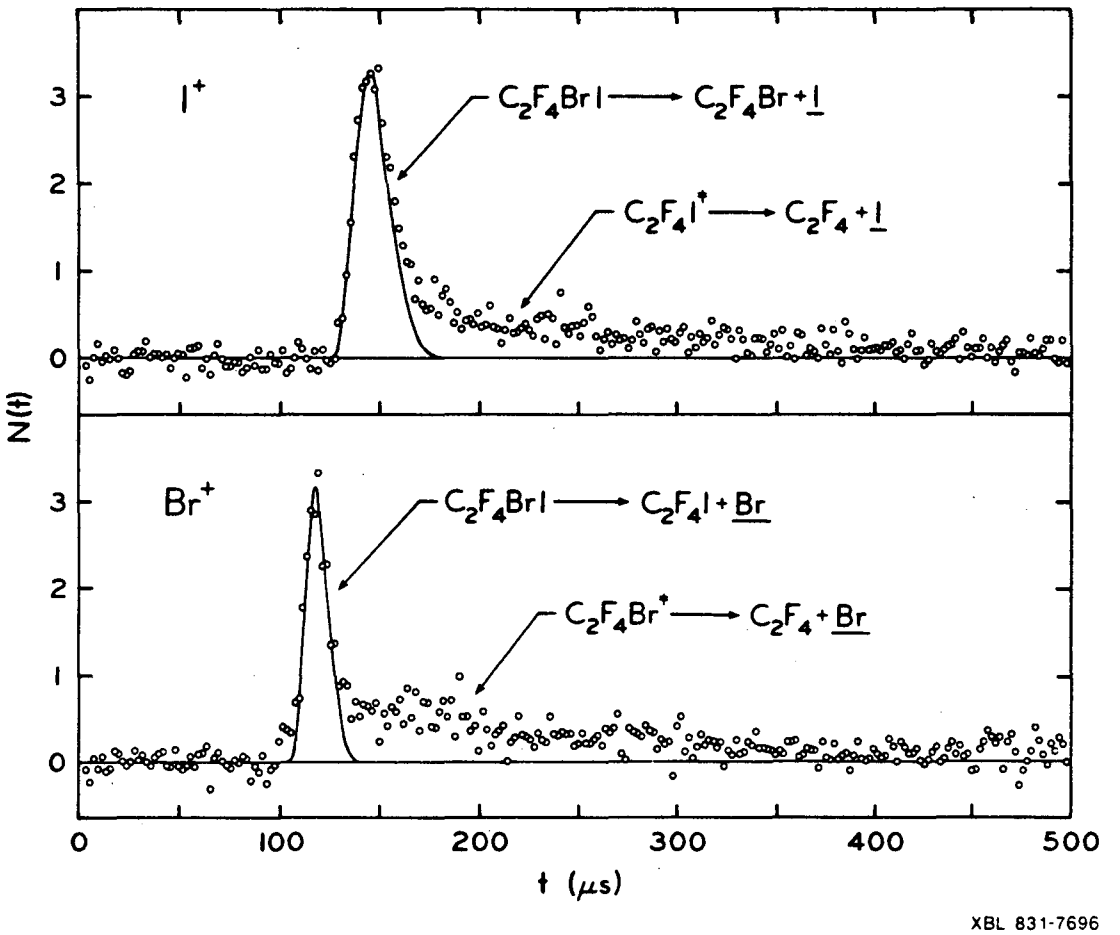
I+
C2F4BrI → C2F4Br + I
C2F4I* → C2F4 + I
Br+
C2F4BrI → C2F4I + Br
C2F4Br* → C2F4 + Br
N(t)
t (μs)
0
100
200
300
400
500
XBL 831-7696

Fig. 15

This report was done with support from the Department of Energy. Any conclusions or opinions expressed in this report represent solely those of the author(s) and not necessarily those of The Regents of the University of California, the Lawrence Berkeley Laboratory or the Department of Energy.

Reference to a company or product name does not imply approval or recommendation of the product by the University of California or the U.S. Department of Energy to the exclusion of others that may be suitable.

TECHNICAL INFORMATION DEPARTMENT
LAWRENCE BERKELEY LABORATORY
UNIVERSITY OF CALIFORNIA
BERKELEY, CALIFORNIA 94720